UCLA
UCLA Electronic Theses and Dissertations

Title
Study of Carbonation and Diffusion in Concrete with Supplementary Cementitious Materials

Permalink
https://escholarship.org/uc/item/5vj6p070

Author
Siu, Jeremy Aidan

Publication Date
2023

Peer reviewed|Thesis/dissertation

eScholarship.org Powered by the California Digital Library
University of California

UNIVERSITY OF CALIFORNIA

Los Angeles

Study of Carbonation and Diffusion in Concrete with Supplementary Cementitious Materials

A thesis submitted in partial satisfaction

of the requirements for the degree Master of Science

in Materials Science and Engineering

by

Jeremy Aidan Siu

2023

© Copyright by

Jeremy Aidan Siu

2023

ABSTRACT OF THE THESIS

Experimental Diffusion Setup for the

Study of Supplementary Cementitious Materials

by

Jeremy Aidan Siu

Master of Science in Materials Science and Engineering

University of California, Los Angeles, 2023

Professor Jaime Marian, Chair

The reduction of carbon dioxide (CO_2) emissions from cement production by the addition of supplementary cementitious materials (SCM's) has garnered significant interest. To predict the CO_2 uptake of systems with SCM's, an experimental setup for measuring the effective diffusion coefficient of CO_2 in concrete was developed. A MATLAB script was written to calculate the diffusion coefficient through curve-fitting of Fick's second law. Six mixtures which represented a ternary binder composition varying in quantity of Portland cement, fly ash, and portlandite were tested after 1, 4, and 7 days of curing. CO_2 uptake was measured by X-ray diffraction (XRD) and thermogravimetric analysis (TGA). Porosity and pore saturation were measured by solvent exchange. Results of the experimental diffusion setup were consistent with these tests, and changes in methods to increase the setup's reliability are discussed.

The thesis of Jeremy Aidan Siu is approved.

Ioanna Kakoulli

Jenn-Ming Yang

Jaime Marian, Committee Chair

University of California, Los Angeles

2023

To my family who has

constantly supported me.

Soli Deo gloria

TABLE OF CONTENTS

LIST OF TABLES

LIST OF FIGURES

LIST OF ABBREVIATIONS

Alite ..... C_3S
Belite ..... C_2S
Calcium silicate hydrate ..... CSH
Carbon dioxide ..... CO_2
Fly ash ..... FA
Isopropyl alcohol ..... IPA
Ordinary Portland cement ..... OPC
Portland cement ..... PC
Portlandite ..... CH
Supplementary cementitious materials ..... SCM
Tetracalcium aluminoferrite ..... C_4AF
Thermogravimetric analysis ..... TGA
Tricalcium aluminate ..... C_3A
X-ray diffraction ..... XRD

ACKNOWLEDGEMENTS

First, I would like to acknowledge Professor Balonis and Professor Abdou, without whose support I would not have made it into this program in the first place. Many thanks also to Uncle Jusson, who has guided me in my engineering endeavors and supported my application to the program.

I would also like to acknowledge the members of LC^2 for allowing me to utilize their facilities for this research. I would like to give special thanks to Dr. Prentice for his tremendous support and patience throughout the year leading to this work. No part of this work would have been possible without him, and I am extremely grateful for all his guidance and assistance. In addition, I would like to acknowledge my committee, Professor Marian, Professor Yang, and Professor Kakoulli, for their work in reviewing this thesis.

Finally, I would like to thank my family for all their love and support, especially during the past five years of my university studies. They have always encouraged me and continue to challenge me to do my best in everything. I cannot express enough thanks for all they have done for me.

CHAPTER 1: INTRODUCTION

1.1: Concrete Carbon Dioxide Emissions

It is estimated that 5-8% of annual carbon dioxide (CO_2) global emissions come from the production of concrete [1]–[3]. Approximately 50% (0.53 $kgCO_2$/kgClinker) of these emissions is from the conversion of limestone ($CaCO_3$) to calcium oxide (CaO), 40% (0.87 $kgCO_2$/kgOPC) is from fossil fuel combustion, 5% is from electricity necessary for manufacturing operations, and 5% is from associated transportation [4]–[6]. From 2015 to 2022, direct emissions remained stable between 0.54 to 0.58 metric tons of CO_2 per ton of cement, but a 3% annual decrease to 0.45 tons CO_2/t cement by 2030 is required to be on track for the Net Zero Emissions Scenario goal for 2050 [7]. Similarly, the thermal energy intensity of clinker for fossil fuels was 3.22GJ/t clinker in 2023, but needs to decrease to 2.68GJ/t by 2030 to be on track for the Net Zero Emissions goal for 2050 [7]. The U.S. annual cement demand is expected to increase from 102 to 119 million tons by 2027 [8]. Approximately 50-60% of carbon emissions in cement production have the potential for reabsorption into the concrete through carbonation [4]. However at ambient conditions, only 18-21% of cement CO_2 emissions are absorbed through carbonation over a 100-year lifecycle, thus the current guidelines for calculating CO_2 emissions (2006 IPCC Guidelines for National Greenhouse Gas Inventories) do not take this carbonation into account, resulting in an overestimation of CO_2 emissions [9], [10].

1.2: Cement Hydration and Carbonation

The hydration reaction of clinker, which is composed of alite (written $3CaO{\cdot}SiO_2$, Ca3SiO5, or C_3S), belite (written $2CaO{\cdot}\ SiO_4$, Ca_2SiO_4, or C_2S), tricalcium aluminate ($3CaO{\cdot}Al_2O_3$, or C_3A), and tetracalcium aluminoferrite ($4CaO{\cdot}Al_2O_3{\cdot}Fe_2O_3$, or C_4AF) to form

calcium-bearing species, including calcium hydroxide ($Ca(OH)_2$, or CH) and calcium silicate hydrates ($3CaO{\cdot}2SiO_2{\cdot}3H_2O$, or CSH) in cement is as follows [11]–[13]:

$$2(3CaO \cdot SiO_2) + 6H_2O \rightarrow 3CaO \cdot 2SiO_2 \cdot 3H_2O + 3Ca(OH)_2$$

$$2(2CaO \cdot SiO_2) + 4H_2O \rightarrow 3CaO \cdot 2SiO_2 \cdot 3H_2O + Ca(OH)_2$$

$$3CaO \cdot Al_2O_3 + 3CaSO_4 \cdot 2H_2O + 26H_2O \rightarrow 3CaO \cdot Al_2O_3 + 3CaSO_4 \cdot 32H_2O$$

$$4CaO \cdot Al_2O_3 \cdot Fe_2O_3 + 10H_2O + 2Ca(OH)_2 + 2(CaSO_4 \cdot 2H_2O) + 18H_2O$$
$$\rightarrow 6CaO \cdot Al_2O_3 \cdot Fe_2O_3 \cdot 2CaSO_4 \cdot 24H_2O$$

The carbonation reactions of the calcium-bearing species including portlandite ($Ca(OH)_2$, or CH), ettringite ($3CaO{\cdot}Al_2O_3{\cdot}3CaSO_4{\cdot}32H_2O$), and calcium silicate hydrate ($3CaO{\cdot}2SiO_2{\cdot}3H_2O$, or CSH) in concrete are as follows [11], [14]:

$$Ca(OH)_2(s) + CO_2(aq) \rightarrow CaCO_3(s) + H_2O$$

$$3CaO \cdot Al_2O_3 \cdot 3CaSO_4 \cdot 32H_2O(s) + 3CO_2(aq)$$
$$\rightarrow 3CaCO_3(s) + 3CaSO_4 \cdot 2H_2O + 2Al(OH)_3(s) + 9H_2O$$

$$3CaO \cdot 2SiO_2 \cdot 3H_2O(s) + 3CO_2(aq) \rightarrow 3CaCO_3 \cdot 2SiO_2 \cdot 3H_2O$$

The presence of water in the pore solution is also necessary for the dissolution of gaseous CO_2 to react with CH [15]. These carbonation and hydration reactions are strongly tied to the properties of concrete. Most notably, the generation of CSH from (in increasing rate) the hydration of C_3S, C_2S, C_3A, and C_4AF leads to an increase in the strength of the concrete [16]. Carbonation also leads to higher mechanical strength due to the lower density $CaCO_3$ precipitates and decrease in porosity [17]. An increase in cement content (and thus an increase in carbonation potential) results in an increase in density and strength, but also an increase in the elastic modulus [18], [19]. The rate of carbonation decreases over time due to formation of a thin

layer of $CaCO_3$ over the surface of CH crystals, thus decreasing the surface area, limiting the rate of reaction, and decreasing the diffusion coefficient of the resulting crystal structure [20].

1.3 Effect of Supplementary Cementitious Materials

Supplementary cementitious (or cementing) materials (SCM's) are waste by-products intentionally added to concrete in replacement of Portland cement (PC) to modify its properties. Some common SCM's include fly ash (FA), which is fine residue produced by coal combustion for thermal power, slag cement, which is formed from the rapid chilling of molten iron blast-furnace slag, and silica fume, condensed from exhaust gases in silicon production [21]. ASTM Standards C61-22, C989-18a, and C1240-20, detail the fineness, permeability, air content, and other specifications for the addition of fly ash, slag cement, and silica fume as SCM's, respectively [22]–[24]. Applications include modification of the rate of strength gain, setting time, permeability, chemical resistance, and economic cost [21], [25]. SCM's have the potential to reduce the net CO_2 emissions associated with concrete both by accelerating the rate of concrete carbonation and by replacing Portland cement as a waste product, thus reducing a concrete mixture's overall emissions. For example, fly ash can decrease CO_2 emissions by 150 kg/m_3 when substituting 50% ordinary Portland cement (OPC) in a 0.5 water to binder ratio [26]. Raw fly ash can absorb up to 180 gCO_2/kg [27]. Complete substitution of Portland cement for fly ash has been shown to significantly increase the carbonation depth by a factor of 2.7 [28].

However, the substitution of OPC for fly ash to reduce emissions compromises early strength gain for later strength gain [29]. Class C fly ash, also known as high calcium fly ash, is primarily comprised of SiO_2, CaO, and Al_2O_3. Standards such as ASTM C618 specify the exact composition of these oxides (see Table 2.6.2) [22], [30]–[33]. After 28 days, a concrete mixture of Portland cement will begin to decrease in the rate of strength gain, eventually increasing in

strength only by approximately 30% after one year. In contrast, a concrete mixture of fly ash and Portland cement will continue to gain strength after 28 days by 50-100% after one year, due to the pozzolanic reaction of silicates and aluminates in the fly ash with portlandite [34].

When replacing Portland cement, fly ash is also used to improve the mixture's workability (ease of pouring while maintaining homogeneity), by decreasing the water needed for the mix and reducing the heat of hydration [29]. Thus, a single SCM has great potential to alter the properties of a mix. Similarly, portlandite which is formed as a result of the hydration reaction of cement may also be introduced at a higher concentration in the initial mixture as an SCM. An abundance of CH would greatly increase the carbonation potential of the mixture due to its high CO_2 uptake at $0.59 g CO_2/g$, more than double that of Portland Cement, and more than triple that of fly ash [35]–[37].

Carbonation is also a function of porosity and diffusivity, as a higher porosity and diffusivity allows CO_2 to penetrate the concrete more easily. Using a wide range of aggregate sizes (e.g., fine sand, coarse gravel) leads to a tighter packing structure and thus more restricted diffusion pathway, leading to a lower diffusion coefficient and decreased carbonation [9]. While the addition of SCM's should theoretically decrease the production of hydrates and lead to a higher porosity and thus permeability compared to pure Portland cement without SCM's, the reality is less clear, as the pore structure has been shown to become more refined with fine pores and fewer coarse capillary pores [30]. A fine pore structure leads to lower permeability, despite a higher porosity. This effect was observed through the addition of slag to Portland cement [38].

However, other effects of SCM's must also be considered, especially mechanical, chemical, and thermal stability. While a larger clinker content ensures higher early strength, it also increases CSH content, which is the most susceptible to carbonation and the risk of leaching

and sulfate attack [39], [40]. Leaching degrades concrete as calcium in the CSH of cement dissolves in water and is replaced by iron through cationic substitution [41]. $MgSO_4$ and Na_2SO_4 solution attacks CSH and increases the silicon to calcium ratio which causes an increase in the rate of expansion by water uptake, ultimately resulting in formation of cracks [42]–[45]. Destruction of CSH by water, $MgSO_4$, and Na_2SO_4 also results in softening and disintegration of the concrete [46].

Corrosion of steel reinforcement in concrete is also a function of carbonation. Dissolution of CO_2 into water pores forms carbonic acid (H_2CO_3), which dissociates into the carbonate ion (CO_3^{2-}) and hydrogen radicals (H^+) [47]. An excess of CH stabilizes the pH above 10.3 but after remaining CH is carbonated, hydrogen radicals accumulate, resulting in a decrease in pH and thus leads to the corrosion of steel [11]. An increase in porosity also increases the rate of this corrosion linearly [48]. Thus, carbonation and hydration of concrete play significant roles in the properties of concrete.

Yet another factor which affects concrete performance is the formation of "secondary" ettringite due to exposure to elevated temperatures. The hydration of $CaSO_4$ and C_3A leads to the formation of ettringite through the following reactions [49]:

$$CaSO_4 \cdot 0.5H_2O + H_2O \rightarrow CaSO_4 \cdot 2H_2O$$

$$3CaO \cdot Al_2O_3 + CaSO_4 \cdot 2H_2O \rightarrow 3CaO \cdot Al_2O_3 \cdot 3CaSO_4 \cdot 2H_2O$$

Ettringite develops in Portland cement as gypsum and sulfates react with calcium aluminate, forming ettringite within hours of adding water, and is thus a function of the availability of sulfates and aluminates in the binder and SCM's [50]. Above a temperature of 70°C (although the exact temperature is not clearly defined), this initially formed "primary" ettringite begins to decompose, and delayed ettringite formation allows "secondary" ettringite to form [50]. Delayed

ettringite formation results in decreased mechanical strength due to cracking, expansion, and decreased bond strength between the binder and aggregate [51]. Thus, the performance of concrete is highly influenced by the addition of SCM's and their effects on carbonation and hydration.

Therefore, to quantify the impact of SCM's on the rate of carbonation, an experimental setup was developed to measure the effective diffusion coefficient of concrete varying in binder composition and curing time. The porosity and pore saturation were measured to determine the effect of the microstructure on diffusion. X-ray diffraction was conducted on samples before and after carbonation to verify changes in carbonation phases. Finally, thermogravimetric analysis was performed to quantify the total CO_2 uptake potential of each mixture.

CHAPTER 2: MATERIALS AND METHODS

2.1: Sample Preparation

Seven mixtures varying in Portland cement (Type I), fly ash (class C), and portlandite (hydrated lime) were prepared, summarized in Table 2.1. However, the M7 samples (portlandite only) lacked adequate mechanical strength for any testing, leaving six mixtures remaining. ASTM C778 graded sand (fine) was used as the aggregate. A water to binder mass ratio of 0.45 was used alongside a binder to aggregate ratio of 0.25 (e.g., for a binder composition of 200g of Portland cement, 90g of H_2O and 800g of sand were used).

Table 2.1: Mass % of binder for each mixture

Mixture	Portland Cement	Fly Ash	Portlandite
M1	33.3%	33.3%	33.3%
M2	50%	50%	-
M3	-	50%	50%
M4	50%	-	50%
M5	100%	-	-
M6	-	100%	-
M7	-	-	100%

Each of the six mixtures were mixed in a stainless steel bowl by hand and with the assistance of a Globe SP05 countertop mixer [52]. Binder and water were mixed together for 30 seconds at 70 rpm followed by the addition of the aggregate, sand. After an additional 60 seconds, the speed was increased to 120 rpm, followed by 60 seconds of mixing by hand with a rubber spatula. Finally, an additional mix followed for 30 seconds at 120 rpm. Each mixture was produced in batches between 1-2 kg. The mixture was then poured and tamped into cylindrical PVC molds of 5 cm diameter and 2.5 cm thickness, which were then sealed with a lid.

Samples of each mixture were prepared and tested after one, four, and seven days of curing. For the diffusion tests, 2-3 samples of each mixture and curing time were tested, and the effective diffusion coefficient was taken as the average of the samples. For the porosity tests, two

samples of each mixture and curing time were tested, and the porosity and pore saturation were taken as the average of the samples. For thermogravimetric analysis (TGA) and X-ray Diffraction (XRD), two samples per mixture and curing time were taken, one of which was from after accelerated carbonation from the diffusion test. Samples were labelled according to their mixture (i.e., "M1" through "M6"), curing time ("C1," "C4," or "C7"), and their carbonation status ("T1" for before carbonation, or "T2" for after carbonation).

2.2: Diffusion Setup

The effective diffusion coefficient of CO_2 in concrete does not simply follow Fick's first law, which assumes that the matrix of diffusion is homogenous and constant with time. This limitation of Fick's first law is well agreed upon [47], [53]–[55]. While Fick's first law may be sufficient for modelling the diffusion of an inert gas, the carbonation of concrete by CO_2 necessitates a more nuanced model. As CO_2 diffuses into concrete, a layer forms where the clinker phases have been completely carbonated, resulting in the formation of $CaCO_3$ (calcite). Beyond this level, CH has undergone carbonation, while CSH remains partially uncarbonated and persists in the layer. Subsequent to this, there exists a region where CH has reacted, and CSH is in the process of decalcification based on the carbonation reactions outlined in Section 1.2 [56]. Each zone exhibits a different gas diffusivity, thus the diffusion coefficient is not only mixture-dependent but also time-dependent as the matrix undergoes change. For this reason, Fick's second law of diffusion is used to reflect the time-dependent nature of the diffusion coefficient:

$$\frac{\partial c}{\partial t} = D\frac{\partial^2 c}{\partial x^2}$$

Figure 2.2.1 shows the experimental setup used for measuring the effective diffusion coefficient. Ultra-high purity compressed nitrogen (N_2) was used as a carrier gas, along with USP medical grade carbon dioxide (CO_2). Prior to each test, the sample was loaded in the sample

holder and the chamber was sealed and purged with nitrogen, and the carbon dioxide sensor (ExplorIR® CM-40831 Development Kit) was calibrated with the GasLab® software. After purging with nitrogen, carbon dioxide was allowed to enter the chamber from the inlet side, and the sensor recorded the concentration of carbon dioxide every two seconds from the reactor outlet. Each test was concluded after the concentration stabilized at a constant value, and a sample was prepared for TGA and XRD analysis.

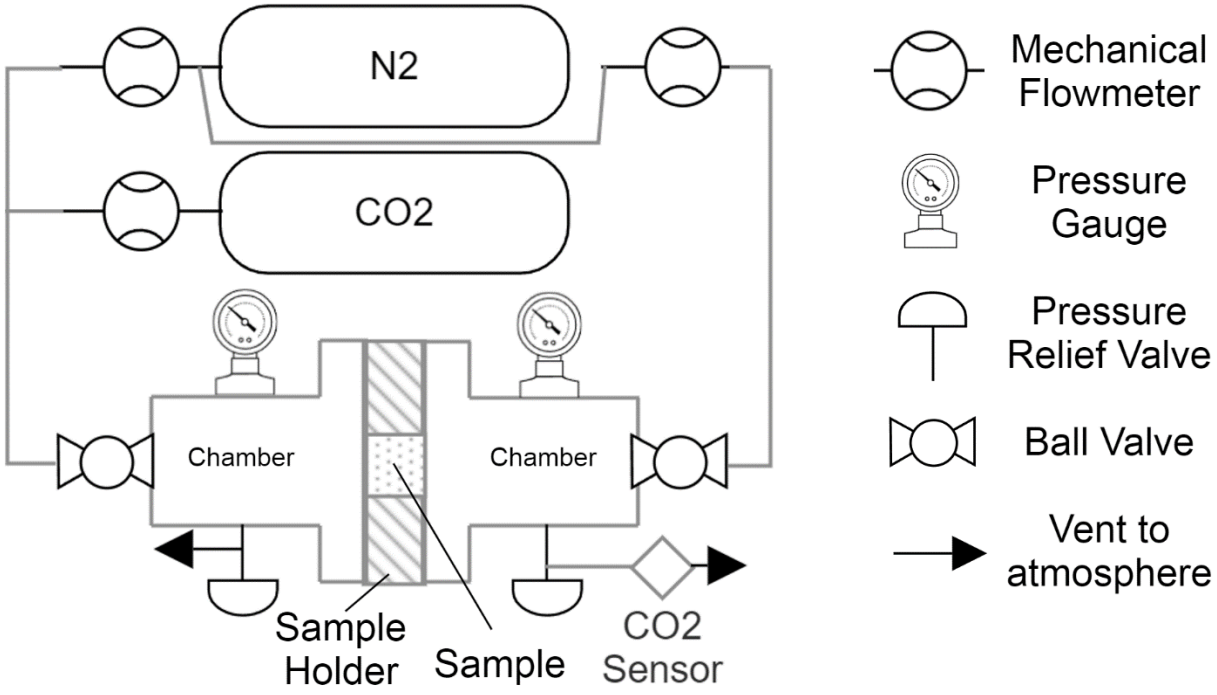

Figure 2.2.1: Schematic of the setup to determine the effective diffusion coefficient

Each half of the diffusion chamber consisted of F316 stainless steel hollow cylinders welded to an ASTM A182-compliant socket-weld flange. The sample holder consisted of discs laser-cut from clear cast acrylic and silicone rubber sheets, as well as silicone rubber gaskets which provided an airtight seal between each half of the chamber when tightened with four evenly spaced steel bolts. The samples were fastened in place through tightening nuts which created an airtight seal with silicone rubber, exposing only opposite faces of the cylindrical

samples. Leaks were assessed by purging the chamber with nitrogen, filling one side with carbon dioxide, sealing the chamber via closing ball valves, and measuring any change in the concentration of CO_2 compared to an atmospheric concentration of 0.04%. Permatrex® 80022 Sensor-Safe Blue RTV Gasket Maker (room-temperature-vulcanizing) was applied between interfaces to ensure a seal between the bolts, nuts, acrylic, and silicone rubber.

Initial testing revealed an error in the preliminary design, where high pressure would accumulate in the inlet half of the chamber, leading to diffusion driven by convection which leads to inaccurate results [57]. Performing the diffusion test in this case led to a diffusion curve which was poorly fit by Fick's law diffusion and an effective diffusion coefficient which was purely a function of the chamber pressure. With this design, the diffusion curve of an empty sample holder was nearly identical to that of a loaded sample holder, as the gas was forced through the sample from sheer overwhelming pressure. Thus, the setup was redesigned and eventually led to the final design shown in Figure 2.2.1, where both halves of the chamber have a gas inlet and pressure relief valves calibrated to the same pressure to minimize any pressure difference between the sides of the sample. A small pressure difference (<1 psi) between each side was still observed. This is likely due to the use of a pressure relief valve rather than a pressure safety valve. A pressure relief valve opens and closes gradually as the threshold pressure is reached, while a pressure safety valve is either opened or closed, with no intermediate state. A pressure safety valve (or membrane manometer [55]) would have been a better design choice in hindsight, however the small remaining pressure difference does not seem to have made a significant impact (see Figure 3.3.1).

The inlet concentration of carbon dioxide is controlled by Key Instruments mechanical flowmeters, and verified with the ExplorIR® sensor, was capable of measuring carbon dioxide

concentration with a resolution of 100ppm, along with the pressure, temperature, and relative humidity. The gas flowrate was measured to be 1.000 SLPM with a digital Alicat Scientific Mass Flow Controller. While simple to set up and relatively inexpensive, one drawback of mechanical flowmeters is the difficulty in controlling the flow consistently. A concentration of 20% CO_2 was calibrated before every test by bypassing the diffusion chamber and connecting the gas canisters to the sensor directly. However, upon connecting the gas canisters back to the chamber and loading a sample, the buildup of pressure on the output side of the mechanical flowmeters led to a decrease in flowrate. This decreased flowrate varied per sample and unevenly between the nitrogen and carbon dioxide flowmeters, leading to a lower concentration of carbon dioxide in the mixture despite the initial 20% calibration. A correction to this design would involve using a pre-mixed source of 20/80% CO_2/N_2, and/or a gas pump prior to the diffusion chamber to force gas in, regardless of the present pressure. In any case, this variation in source carbon dioxide concentration was taken into account when calculating the effective diffusion coefficient and did not impact the resulting value (see Figure 3.3.2).

2.3: Measurement of Porosity and Pore Saturation

For a material of high diffusivity, a high porosity and low pore saturation are expected. The porosity and pore saturation of each sample was determined through the solvent exchange method. Each sample was removed from its mold, then weighed and soaked in IPA for 24 hours to arrest hydration. Following this, each sample was dried in an oven at 105°C for 24 hours, and then weighed. Each sample was then soaked in IPA for another 24 hours and weighed.
The porosity, ϕ, and water pore saturation, S, was calculated according to the following equations:

$$\phi = \frac{Volume\ of\ Pores}{Volume\ of\ Sample}$$

$$= \frac{(M_s - M_d)/\rho_{IPA}}{M_m/\rho_m}$$

$$S = \frac{Volume\ of\ Water}{Volume\ of\ Pores}$$

$$= \frac{(M_m - M_d)/\rho_{H2O}}{(M_s - M_d)/\rho_{IPA}}$$

M_m is the sample mass after curing, M_d is the mass after oven drying, M_s is the mass after IPA saturation, ρ_{H2O} is the density of water, ρ_{IPA} is the density of IPA, and ρ_m is the density of the mixture, tabulated in Table 2.3:

Table 2.3: Density of mixtures and their components for porosity and saturation calculations

Mixture	Theoretical Density ρ_m (g/cm^3)	Component	Density (g/cm^3)
M1	1.656	Portland Cement	3.14
M2	1.709	Fly Ash	2.75
M3	1.616	Portlandite	2.21
M4	1.655	Sand	1.4
M5	1.748	IPA	0.786
M6	1.670	Water	1

In solvent exchange, a solvent miscible with water such as acetone, ethanol, methanol, or in this case, isopropyl alcohol (IPA) is used to replace the concrete pore solution. By replacing the pore solution, hydration within the cement is arrested, and the sample can be dried via vacuum or elevated temperature. Zhang and Scherer compared various other methods for the hydration of cement, each with their advantages and drawbacks [58]. Unfortunately, all current drying techniques were found to have a deleterious effect on the concrete structure due to the dehydration of CSH and ettringite [58]. For example, oven drying at 105°C and atmospheric pressure was found to alter the pore structure, resulting in a more coarse pore size distribution (radius > 50 nm) [59]. Through solvent replacement with IPA, the resulting pore distribution was

more fine (radius <25nm), but can result in chemical artifacts due to reaction between the solvent and hydration reaction products [58], [59]. Taylor and Turner confirmed these findings and concluded that organic liquids could not be removed with vacuum drying or elevated temperatures without significantly changing the structure due to the strong bonding between organic liquids and surface C_3S [60]. Still, it has been concluded that solvent replacement with IPA as the solvent is the best method for studies which require the fine pore structure to be maintained/preserved, while direct oven drying without solvent replacement of the water in pore solution caused damage to pore structure.

One difficulty with the method used in this experiment was due to the brittleness of tested samples, particularly those with high portlandite and low Portland cement portions, such as M3 (50/50% CH/FA). Removing the sample from the mold sometimes induced significant stress that caused the sample to crumble. Even after removal from the mold, some samples had the tendency for small pieces to flake off like dust while being handled and while soaking in IPA. This may have led to inaccurate measurement of the porosity and pore saturation. Furthermore, the equations for calculating the porosity are rather simplified and do not consider the intricacies between open pores (exposed, on the sample surface) vs. closed pores (beneath the sample surface). A more precise measurement could have been taken if, for example, the bulk volume was calculated from the submerged mass using Archimedes' principle, rather than the mass after curing and theoretical density.

2.4: Powder Preparation

Two samples of each mixture and curing time were prepared for TGA and XRD tests. Powder from samples was obtained with a drill press, then ground with a mortar and pestle and put through a No. 50 sieve for 300 μm according to ASTM E11 guidelines for woven wire test

sieves [61]. The powders were then transferred to plastic test tubes and soaked in IPA to arrest hydration, followed by an initial oven dry at 50°C for 24 hours, and a final dry under vacuum. Ideally, all drying would occur under vacuum so that risk of carbonation is minimized. However, due to the large number of samples and the time associated with drying, an initial oven-dry at 50°C was used to remove excess IPA before the final dry in vacuum. Due to apparatus availability, samples that could not be immediately tested for TGA or XRD on their exact curing day (1, 4, or 7 days) were simply stored in vacuum until testing.

2.5: Thermogravimetric Analysis

Thermogravimetric analysis (TGA) was performed in order to measure the CO_2 uptake and thus carbonation potential of each mixture over time. For every sample, between 10-30 mg were loaded into the crucible for TGA. Ultra-high purity compressed nitrogen (N_2) was used as the inert gas, at a pressure of 1.9 bar and flow rate of 19.8 mL/min. Each sample was heated to 50°C and held for 5 min, then heated further to 950°C at a rate of 15°C/min. A PerkinElmer Simultaneous Thermal Analyzer (STA) 6000 was used to conduct the test.

The carbon dioxide uptake for each sample was determined according to the following formula:

$$\%CO_2 = (m_{950°C} - m_{550°C})_{T2} - (m_{950°C} - m_{550°C})_{T1}$$

The difference of the mass of the post-diffusion sample (denoted by "T2") between 550°C and 950°C, compared to that of a sample before diffusion (denoted by "T1"). Between this temperature range is the decomposition of calcium carbonate into calcium oxide and carbon dioxide ($CaCO_3 \rightarrow CaO + CO_2$), and thus is directly proportional to the absorption of carbon dioxide within the sample [62]. The change due to accelerated carbonation from the diffusion test

can thus be measured between the two samples. The temperature bounds were determined based on the TG curve, as well as the derivative of the TG curve (dTG) [63]–[66].

2.6: X-ray Diffraction and Materials Characterization

To observe changes in cement phases due to carbonation, X-ray diffraction was performed on each sample. Each sample was tested between 5-50° 2θ, at increments of 0.02° 2θ. XRD was also tested on the raw components: Type I Portland cement, Class C Fly Ash, synthetic portlandite, and fine sand, shown in Figure 2.6.

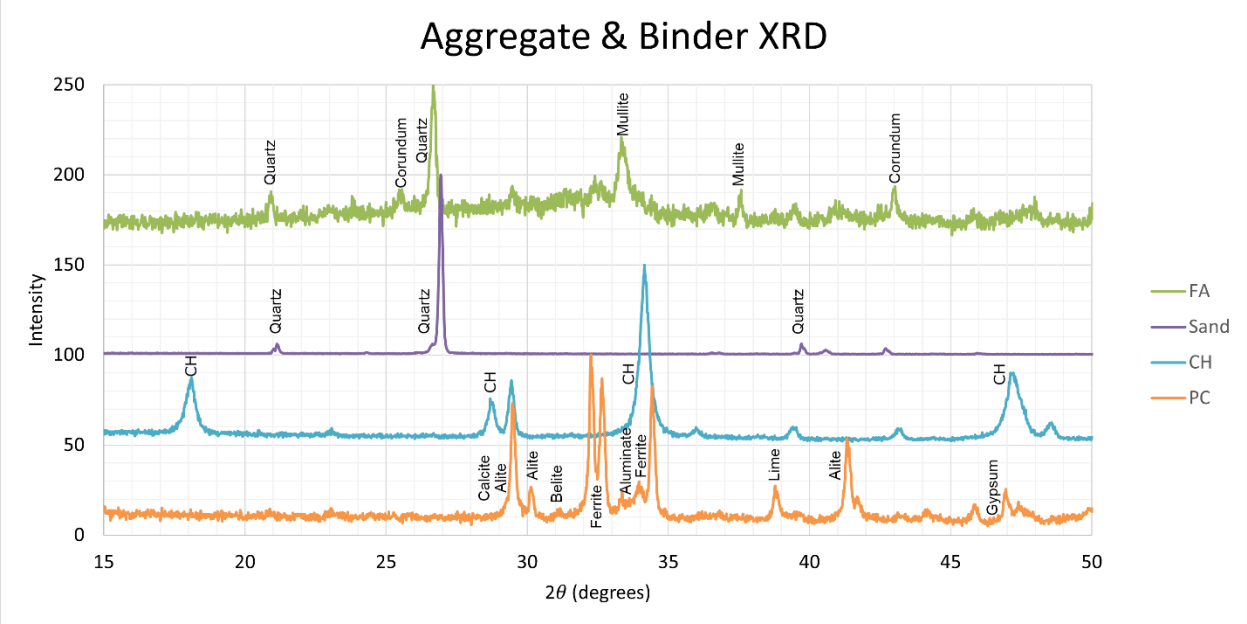

Figure 2.6: XRD of fly ash (FA), sand, portlandite (CH), and Portland cement (PC).

ASTM C-150 specifies the composition for Type I Portland cement, summarized in the Table 2.6.1 [51], [67]. Type I Portland cement is considered general purpose, while other types such as Type II and III specialize in sulfate resistance and high early strength, respectively.

The following phases of significance were identified for the XRD of Portland cement at corresponding angles of 2θ: calcite at 29.48° [68]; alite at 29.52°, 30.17°, and 41.3°; ferrite at 34.4° and the ranges of 32.26° to 32.30°, and 32.61° to 32.66° [68]; aluminate at 33.36° [68],

[69], belite at 31.14° [68], [69], and lime at 38.78° [68]. The magnitude of the XRD peak intensity is indicative of the amount of corresponding phase present. For example, it has been found that the peak intensity of alite has a logarithmic relationship with the amount present [68], [69]. Relative to belite, alite has a much higher concentration in ordinary Portland Cement clinker, leading to higher peaks of alite and much lower (barely distinguishable, in this case) peaks of belite [68].

Table 2.6.1: Composition of Type I Ordinary Portland Cement

Species	**Amount**
CaO	60% min.
SiO_2	20% min.
Al_2O_3	6% max.
Fe_2O_3	6% max.
MgO	6% max.
SO_3	3% max.
Clinker (phase)	**Amount**
C_3S (alite)	50-70%
C_2S (belite)	10-20%
C_3A (tricalcium aluminate)	8-10%
C_4AF (tetracalcium aluminoferrite)	5-15%
$C\bar{S}H_2$ (gypsum)	3-4%

ASTM C618 specifies properties for class C fly ash such as maximum moisture content (3% max.), loss on ignition (6% max.), and composition [22], [30]–[32]. The composition requirements of ASTM C618 class C fly ash are summarized in Table 2.6.2.

Table 2.6.2: Composition of class C fly ash

Species	**Amount**
$SiO_2 + Al_2O_3 + Fe_2O_3$	70% min.
CaO	18% min.
SiO_3	5% max.
SO_3	5% max.

The following major phases were identified for the XRD of fly ash at corresponding angles of 2θ: Quartz (SiO_2) at 20.9° and 26.7° [70], mullite ($2Al_2O_3\ SiO_2$) at 33.4° and 37.5°

[70], corundum (Al_2O_3) at 25.6° and 43.0° [71], and gypsum ($CaSO_4 \cdot 2H_2O$) at 45.9°, 47.0°, and 47.6° [72]. The amorphous hump between 28° to 35° 2θ represents aluminosilicate glasses which play a large role in the reaction mechanisms of fly ash in cement systems [70]. The exact composition and phases of this region have been researched extensively in other studies [73]–[80].

ASTM C207-18 details the specifications for hydrated lime to be added to Portland cement concrete [81]. The intensity peaks at 18.11°, 28.78°, 29.47°, 34.15°, and 47.24° 2θ are all consistent with characteristic peaks of portlandite ($Ca(OH)_2$) [82]. The peaks for sand (ASTM C778) at 21.13°, 26.93°, and 39.71° are consistent with those of quartz (SiO_2) [83]. These quartz peaks were present in all the mixture materials.

CHAPTER 3: RESULTS AND DISCUSSION

3.1: X-ray Diffraction

The X-ray Diffraction for all six mixtures is shown in Figure 3.1.1 and 3.1.2, grouped by mixture, curing time, and carbonation state (before or after diffusion). The following peaks were identified with their phases labelled (where applicable) on each graph: CH at 18.1°, 34.3°, 36.6°, and 47.3°; Calcite at 29.5°, and Quartz at 20.9°, 26.6°, 39.6°, 40.4°, and 42.6°.

For Portland cement samples (M1, M2, M5) a decrease in the clinker phases, including alite, belite, aluminate and ferrite, was expected and observed for all samples. This is according to the hydration reactions of calcium silicates into CH, and CSH. Thus, an increase in portlandite, ettringite, and amorphous phase content was also expected with increased age [16], [68], [84]. There may be peaks located around 9.0° (not shown in Figure 3.1.1 or 3.1.2), 15.5°, and 32.0° 2θ which indicate the presence of ettringite [27], [85], [86], but it is difficult to quantify the presence of ettringite due to the overlap of peaks with CSH [84], [87], and peaks were not clearly observed by visual inspection.

Table 3.1: X-ray diffraction peaks for each mixture

Phase	Angle (2θ)
Portlandite	18.1°
Quartz	20.9°
Quartz	26.6°
Calcite	29.5°
Portlandite	34.3°
Portlandite	36.6°
Quartz	39.6°
Quartz	40.4°
Quartz	42.6°
Portlandite	42.6°

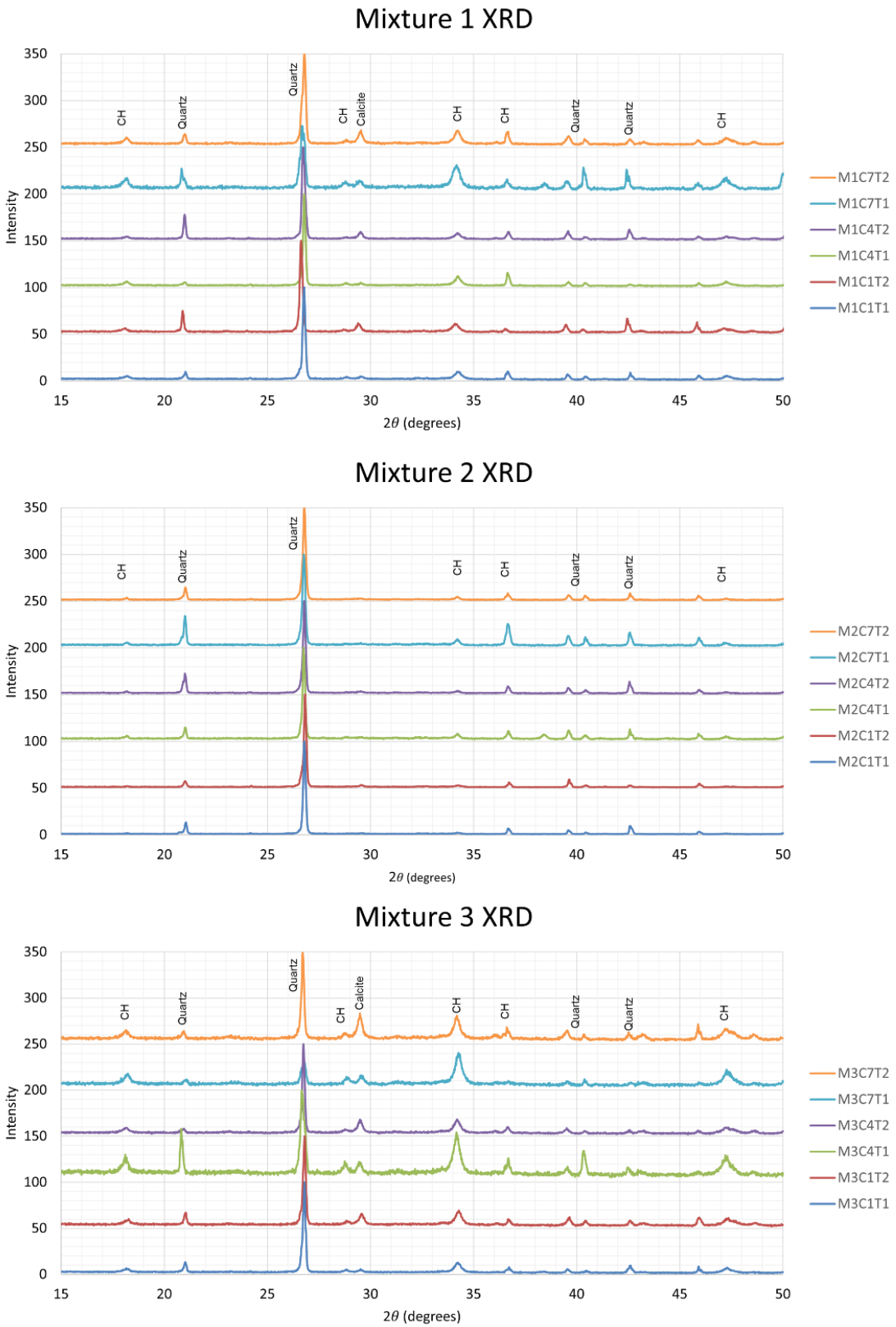

Figure 3.1.1: XRD for the mixtures M1, M2, and M3, from 15° to 50° 2θ

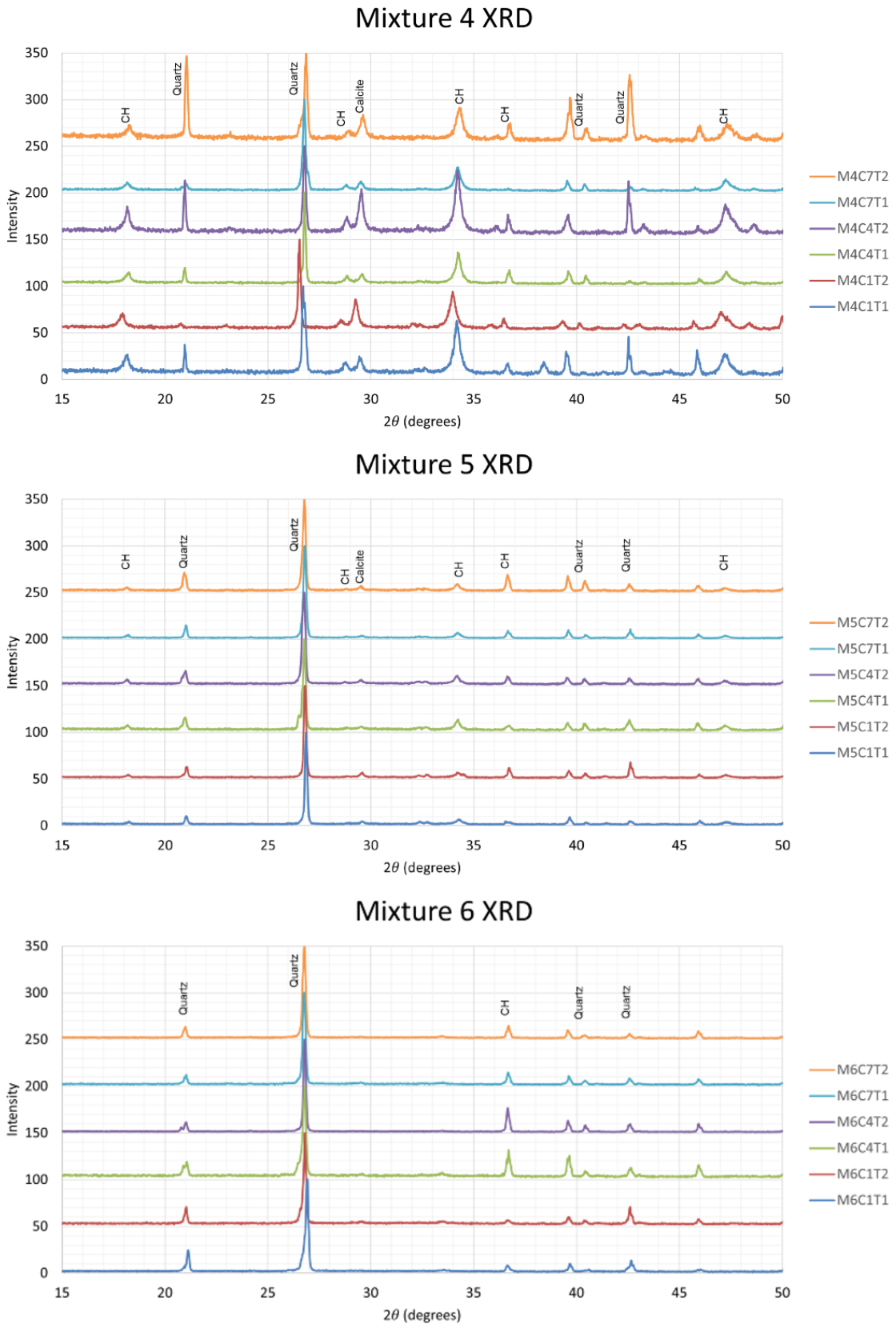

Figure 3.1.2: XRD for the mixtures M4, M5, and M6, from 15° to 50° 2θ

The content of CH was indeed found to increase over time due to the hydration reaction of clinker phases, though the exact amount was not determined as no XRD quantitative analysis was performed [16], [68], [84]. In contrast, the CH content was expected to decrease for samples tested after diffusion due to the carbonation of CH forming $CaCO_3$ [56]. This expectation was confirmed in the decrease of XRD peak intensities of CH and quantified in TGA results (see Section 3.2]. In samples initially mixed with high portlandite content (M1, M3, M4), notably large increases in the calcite content were observed after carbonation at 29.5° 2θ. This is to be expected due to the carbonation of CH. This increase is also seen on a much smaller scale in M5, likely due to the high content of Portland cement in the original mixture leading to clinker hydration and the formation of calcite. M4, which was mixed with the highest content of CH and Portland cement, also had the highest peaks of CH and calcite. M2 (50/50% FA/PC) and M6 (100% FA) primarily exhibited quartz peaks due to the high quartz content in both sand and class C fly ash from the original mixture [30].

Against expectations, M4 also had large CH peaks at 4 days of curing, after carbonation, at 18.1°, 34.3°, and 47.3° 2θ. This may be explained in conjunction with its exceptionally low effective diffusion coefficient: the method for carbonating samples relied upon the diffusion test reaching a steady CO_2 outlet concentration. Generally, samples with a higher diffusion coefficient reached a steady value more quickly than those with a lower diffusion coefficient, which took longer and had a lower inlet CO_2 concentration due to the pressure buildup at the mechanical flowmeters (discussed in Section 2.2). Samples were expected to have undergone nearly equal levels of carbonation by the end of each respective test, but this assumption is unsupported and may have led to different degrees of carbonation for certain samples, such as M4 at 4 days of curing. In hindsight, it is clear that a more consistent carbonation method would

have benefited the accuracy of these results. Despite this anomaly, it can be seen that carbonation generally resulted in a decrease of CH and the formation of calcite (for CH-rich samples).

3.2: Porosity and Pore Saturation

The porosity and pore saturation degree of each sample was graphed in Figure 3.2.1 and 3.2.2 as a function of the curing time, respectively. However, the difference observed in the samples' porosity over the 7-day period was relatively small: M1 fluctuated between 19.6% and 23.7%; M2 decreased from 13% to 12%; M3 increased from 21.8% to 25.2%; M4 fluctuated between 28.2% and 25.3%; M5 fluctuated between 15.8 and 15.0%; lastly, M6 remained steady between 14.5% and 14.6%.

Due to the low number of samples, it is difficult to ascertain whether the measurements taken were precise enough to indicate a statistically significant change. It is possible that a longer curing time or more robust sample preparation methods were necessary to observe greater change over this short period of time. For example, the time required for each sample for solvent exchange was assumed to be no greater than 24 hours based on similar methods, but incomplete solvent exchange which required more than 24 hours could have adversely impacted measurements [58], [88]. If more time was available, each sample could continue to be soaked and weighed on a daily basis until a constant weight was reached. Alternatively, the temperature of the solution could have been elevated to increase the rate of solvent penetration and reduce the required soaking time [89].

The pore saturation of concrete is the volume fraction of pores occupied by water. When water was added in the initial binder mixture, a value close to 100% pore saturation was expected. A pore saturation less than 100% indicates the presence of empty pores (filled only with air). However, as seen in Figure 3.2.2, the pore saturation varies widely, with values as low

as 32% and as high as 98%. This is likely due to poor packing of the samples as mixtures were dry from the high aggregate to binder ratio, and manual compaction of the mixtures into molds was inadequate in removing empty pores.

The observed trend is instead that the pore saturation was dependent on the mixture. This is more clearly seen in Figure 3.2.3, where each mixture is clustered around similar pore saturation and porosity values. M6 (100% FA) and M2 (50/50% FA/PC), which were expected to have the highest moisture from their high fly ash content, exhibited the highest pore saturation between 80-100% and 75-85%, respectively.

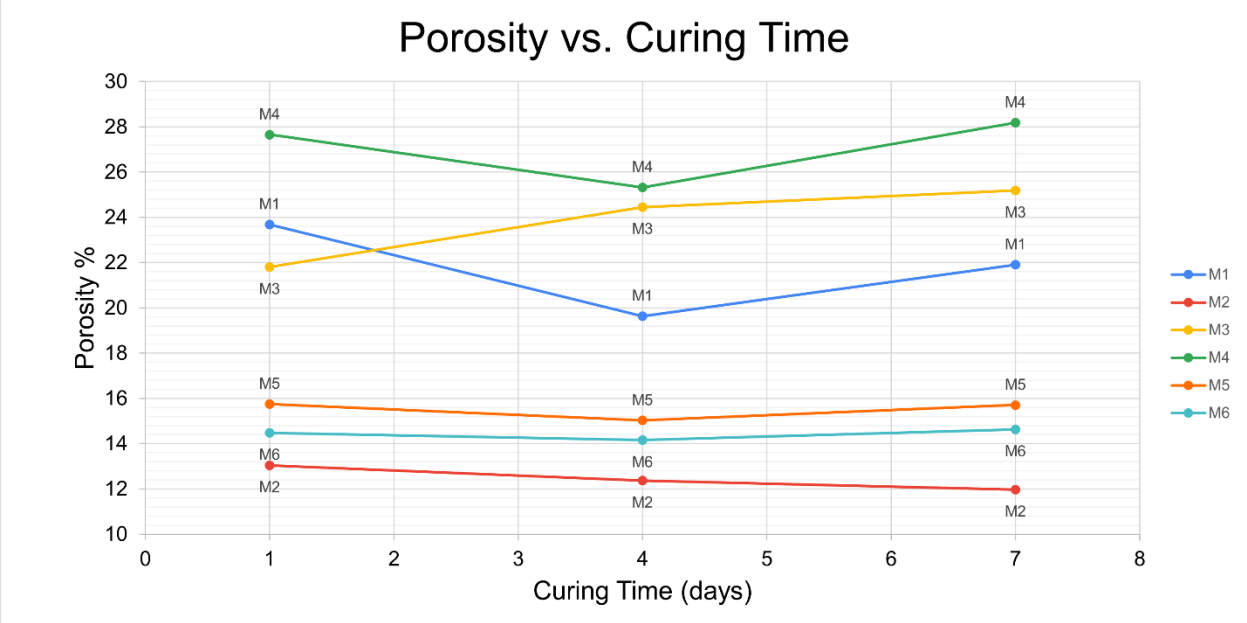

Figure 3.2.1: Average porosity of each sample after 1, 4, and 7 days of curing

Mixtures with high portlandite content in the original mix (M1, M3, M4) had the lowest pore saturation, increasing with fly ash content (to a greater degree) and Portland cement content (to a lesser degree). That is, a mixture of portlandite and Portland cement (M4) was expected and is observed to have the lowest pore saturation. It is likely that in order to achieve a pore saturation near 100%, a higher water to binder ratio is required, especially for mixtures with portlandite in the original mixture.

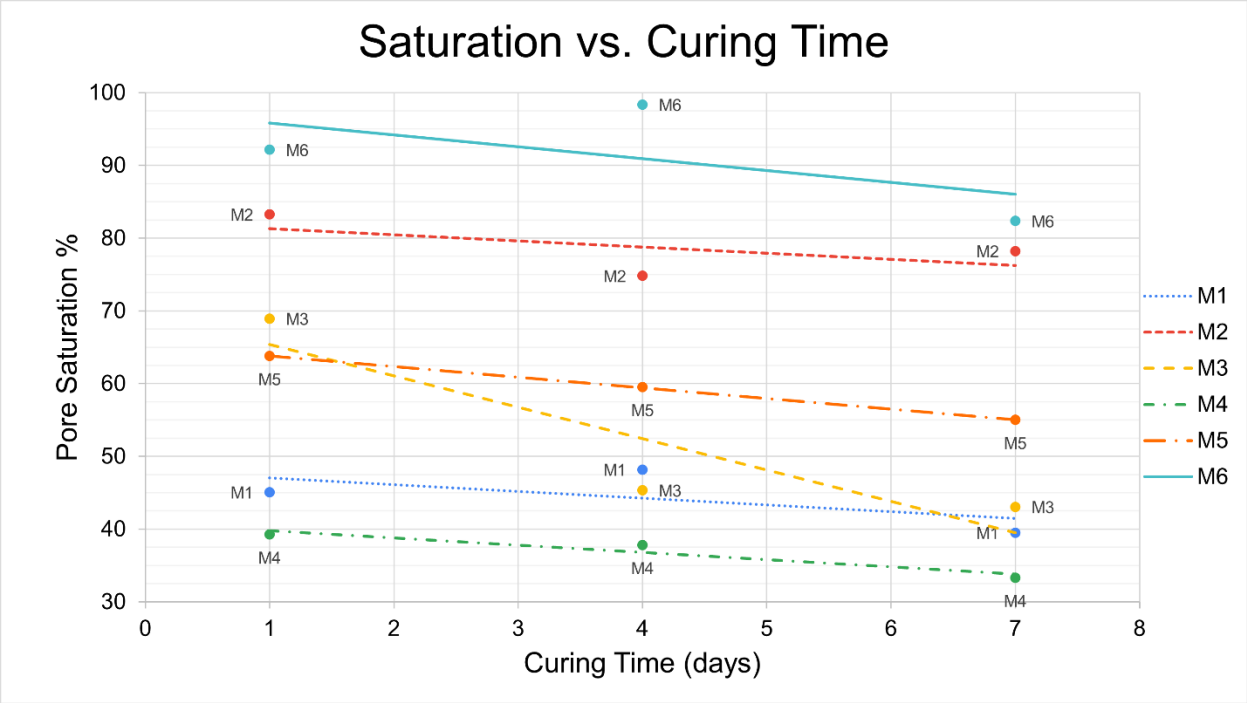

Figure 3.2.2: Average Pore Saturation of each sample after 1, 4, and 7 days of curing

Small differences were observed in the pore saturation degree for each mixture over the 7-day period. Overall, each mixture exhibited a decline in pore saturation over time. This trend is to be expected due to the continued hydration reaction over time and thus decrease in pore water content. However, within the 7-day period examined, the pore saturation is more dependent on the mixture as seen in Figure 3.2.3. Each mixture clusters around a certain porosity and pore saturation degree, indicating that the porosity and pore saturation are primarily a function of the mixture composition more than any other factor such as curing time. Overall, an inverse relationship was observed between the porosity and the pore saturation. This inverse linear relationship supports the proposition that the pore saturation degree was limited by the overall water content. As the porosity decreases, the volume of saturated pores may not necessarily increase, but the volume of empty pores does decrease, thus increasing the pore saturation degree.

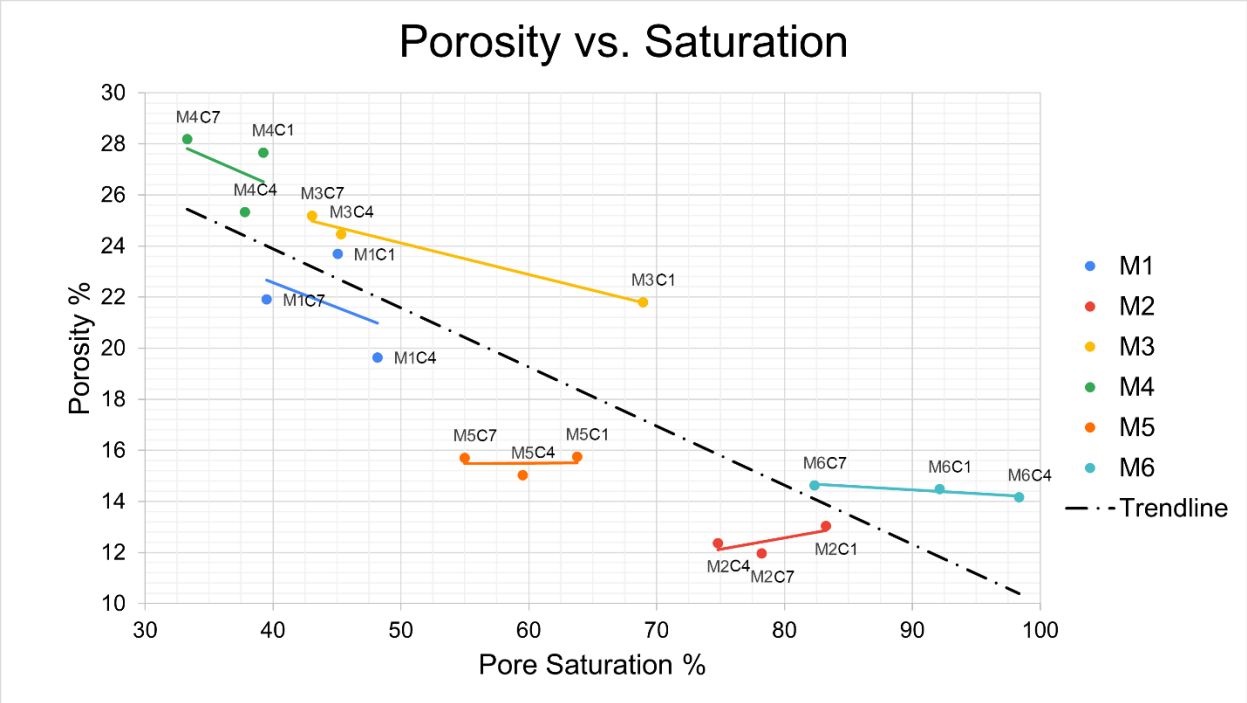

Figure 3.2.3: Porosity vs. Saturation for each sample after 1, 4, and 7 days of curing

3.3: Effective Diffusion Coefficient

Prior to diffusion testing of the samples prepared in Section 2.1, the experimental setup for diffusion was verified by testing samples of 1-day cured PC concrete (of the same composition as M5 in Table 2.1) varying in thickness between 2 to 5 cm. As seen in Figure 2.2.2, there is little variation in the effective diffusion coefficient over the range of sample thicknesses. Over 9 samples, an average and standard deviation of 1.263E-6 m^2/s and 2.498E-7 m^2/s was observed, respectively. Needless to say, the diffusion coefficient is a function of the composition of the sample. For a similar composition utilizing a water to binder ratio of 0.45 with Portland cement, fine sand, and gravel after 1 day of curing, Yoon and Chang found a slightly lower diffusion coefficient between 0.6E-6 m^2/s to 1.0E-6 m^2/s [90]. A lower diffusion coefficient is to be expected, as a wider range of aggregate sizes leads to a tighter packing structure and thus a more restricted diffusion pathway [9].

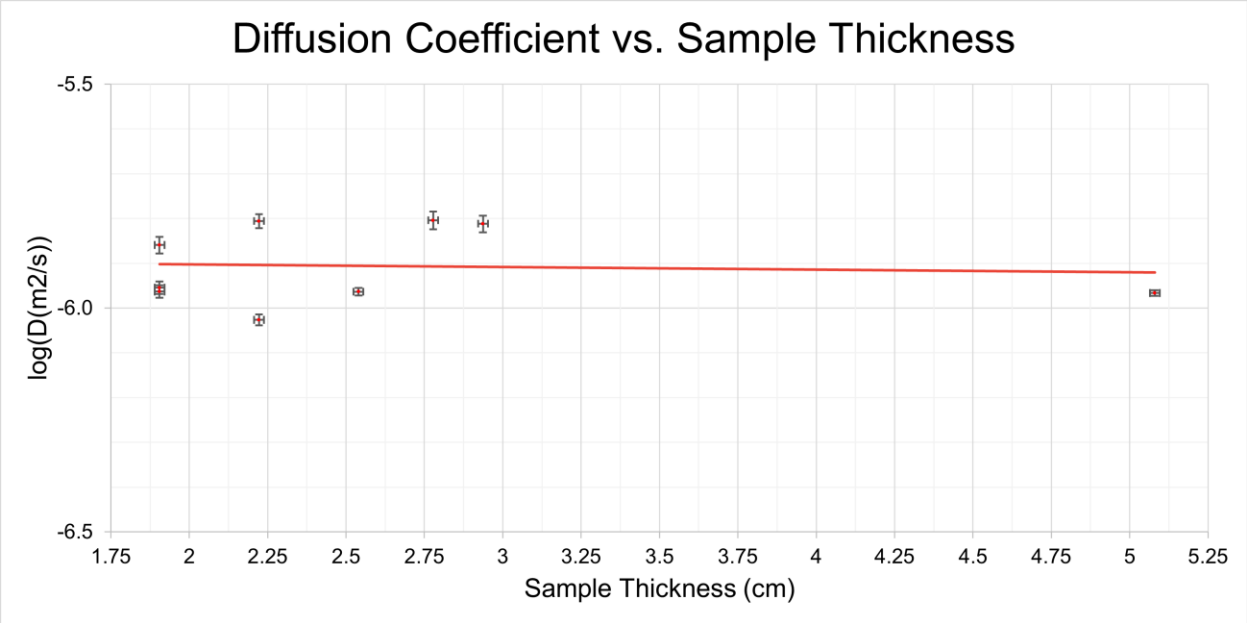

Figure 3.3.1: Plotting the logarithm of the effective diffusion coefficient vs. sample thickness shows a near-constant (0-slope) value, as is expected for samples of the same mixture composition.

The delay in the increase of carbon dioxide concentration is demonstrated in Figure 3.3.2. For the same mixture, as the thickness of the sample increased, the curve is flattened and shifted toward the right, indicative of the delay due to the gas taking a longer path before reaching the sensor.

To calculate the effective diffusion coefficient from the curve of concentration vs. time, a MATLAB program was written to fit a solution of Fick's second law to the curve. The infinite source, semi-infinite bar 1-D solution to Fick's second law is as follows [91]:

$$C(x,t) = C_0 + (C_b - C_0)\mathrm{erf}\left(\frac{x}{2\sqrt{Dt}}\right)$$

C is the concentration, *x* is the position relative to the sample surface at the source, *t* is time, *D* is the diffusion coefficient, and erf is the Gauss error function. This solution has the following boundary conditions:

$C_x = C_b$ for $t = 0$ and $x > 0$;

$C_x = C_0$ for $t > 0$ and $x = 0$;

$C_x = C_x$ for $t = t$ and $x = x$.

Thus, the following assumptions are made: (1) the initial bulk concentration, C_b, is constant throughout the entire length of the sample at $t = 0$; (2) the source concentration, C_0, is constant at the surface $x = 0$ throughout time $t > 0$; (3) the concentration, C_x, is a function of time and position. Utilizing the Curve Fitting Toolbox for MATLAB and knowing the thickness of the sample, the diffusion coefficient can be calculated from fitting the curve of concentration vs. time to this solution of Fick's second law.

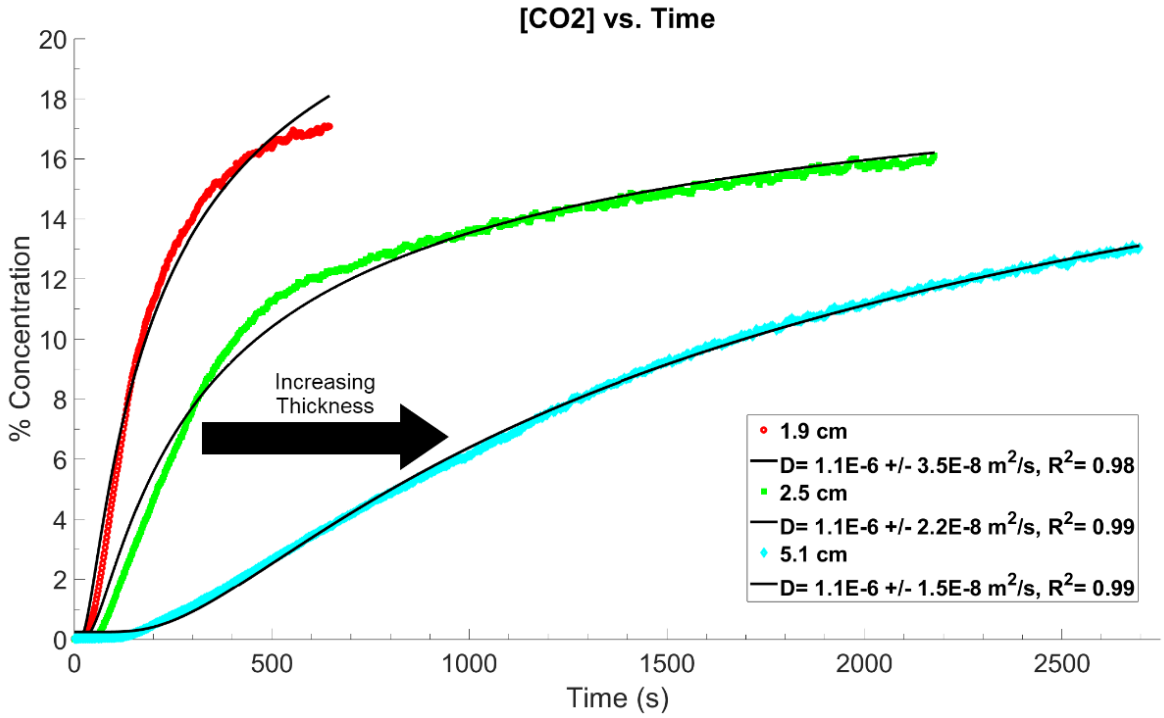

Figure 3.3.2: The diffusion curves for one mixture, three samples of varying thickness.

For three samples of thickness 1.9 cm, 2.5 cm, and 5.1 cm, the diffusion coefficient remained constant at 1.0890 m^2/s, 1.0876 m^2/s, and 1.0755 m^2/s, respectively. The R^2 value was also very high at 0.9876, 0.9914, and 0.9939, respectively, indicating a good fit. The +/- error for

each coefficient was also calculated from the Curve Fitting Toolbox based on the 95% confidence interval and was 2 orders of magnitude less than the diffusion coefficient for these samples, as well as for nearly all other samples.

The curve-fitting program written in MATLAB was used to fit a diffusion curve to the graph of concentration vs. time for each sample. An example of the fitting is shown in Figure 3.3.3 to demonstrate the ability to fit the curve over multiple orders of magnitude of the effective diffusion coefficient. The high R^2 value above 0.97 indicates a good fit.

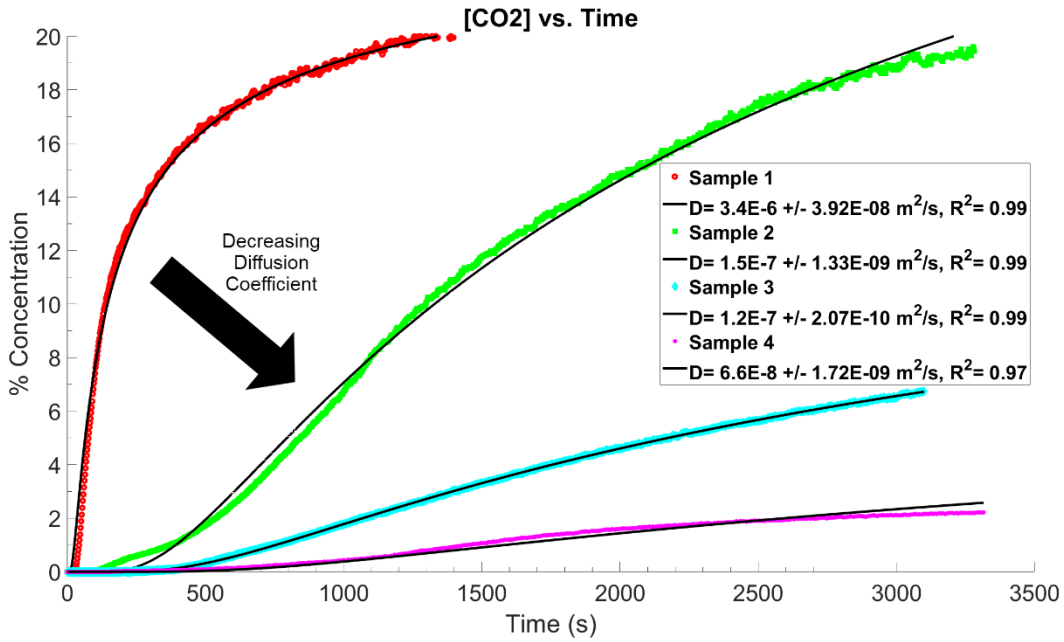

Figure 3.3.3: Example of fitting the diffusion curve over multiple orders of magnitude.

The diffusion coefficient is expected to decrease with an increase in carbonation. The effect of the precipitation of $CaCO_3$ through carbonation of $Ca(OH)_2$ to clog pores and thus decrease gas diffusivity has been well documented [47], [92]–[98]. This was verified with the diffusion setup by performing the diffusion test multiple times on a sample (PC), effectively measuring the diffusion coefficient before and after carbonation, and the decrease in diffusivity was indeed observed (Figure 3.3.4). Therefore, mixtures with more calcium-bearing species such

as portlandite, which has the highest carbonation potential out of Portland cement and fly ash, will have the lowest diffusion coefficient, while fly ash which has the lowest carbonation potential will have the highest diffusion coefficient. This carbonation potential is discussed further in Section 3.4.

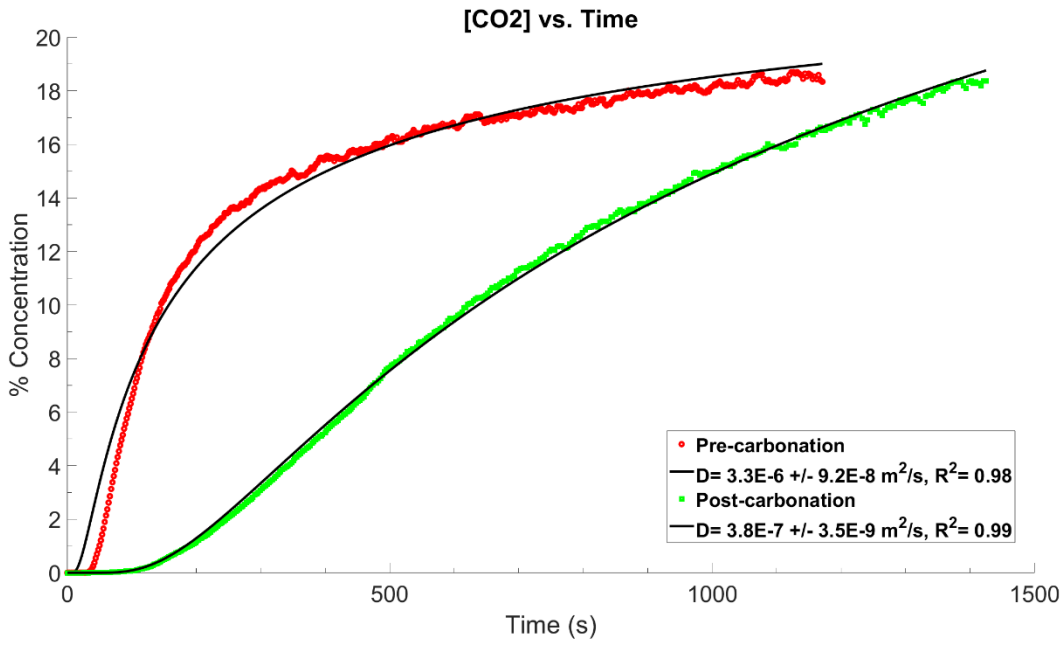

Figure 3.3.4: Diffusion curves for a sample before and after its first diffusion test

The effective diffusion coefficient of carbon dioxide through each mixture is visualized in Figure 3.3.5. The coefficient is expected to increase with porosity, as a greater porosity allows for a less tortuous path and thus increased diffusivity [55]. In contrast, an increase in the pore saturation of a sample is expected to decrease the coefficient because the diffusivity of CO_2 through water (between 1.6E-9 m^2/s to 1.9E-9 m^2/s) is much lower compared to its diffusivity through air/empty pores (1.6E-5 m^2/s) [47], [99]–[101]. Therefore, mixtures with more fly ash which have higher pore saturation (and thus low porosity, as discussed in Section 3.2) will have lower diffusivity, while mixtures with more portlandite (low pore saturation, high porosity) will have higher diffusivity.

This ultimately leads to a disagreement between the expected behaviors of each component. Based on its high porosity and low pore saturation (Figure 3.2.3) Portlandite is expected to exhibit the highest diffusivity. However, based on its high potential for carbonation (see Figure 3.4), Portlandite is expected to exhibit the lowest diffusivity. Similarly, fly ash is expected to exhibit a low diffusivity due to its low porosity and high pore saturation. However, its low carbonation potential suggests that it could also exhibit high diffusivity [20], [47], [102]. Some research has shown that an increase in fly ash decreases the diffusion coefficient overall, while other research has shown that for a water to binder ratio of 0.25, the diffusion coefficient increased with increasing fly ash content if the fly ash content exceeded a threshold of 45% [54], [103], [104]. Thus, due to the complexity of the system, it should be noted that the following discussion may potentially be limited to the specific mixtures and methods outlined in this study.

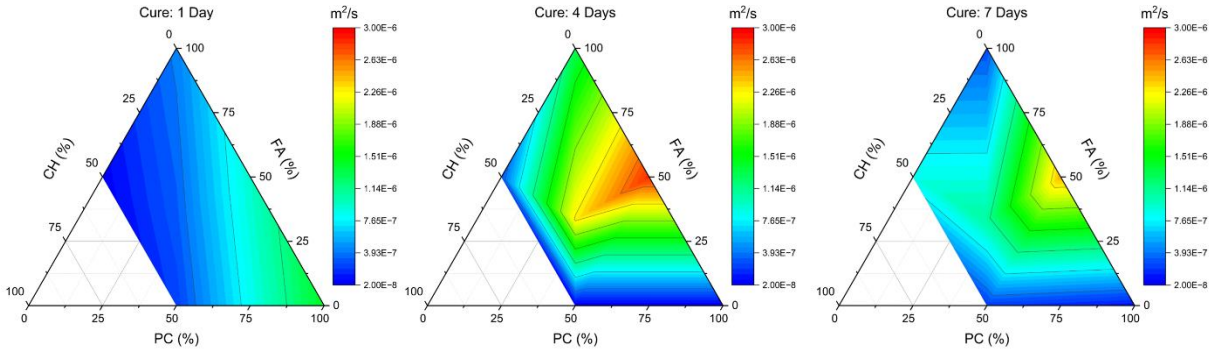

Figure 3.3.5: Ternary contour plot of the effective diffusion coefficient

After 1 day of curing, the mixtures high in Portland cement, M5 (100% PC) and M2 (50/50% PC/FA), had the highest effective diffusion coefficients at 1.45E-6 m^2/s and 9.50E-7 m^2/s, respectively. The mixtures high in portlandite, M4 (50/50% CH/PC) and M3 (50/50% CH/FA), had the lowest effective diffusion coefficients at 2.32E-7 m^2/s and 4.20E-8 m^2/s, respectively. Mixtures M6 (100% FA) and M1 had effective diffusion coefficients of 4.20E-7 m^2/s and 3.08E-7 m^2/s, respectively.

This suggests that the carbonation of portlandite had the greatest contribution to the decrease in diffusion coefficient for M1, M3, and M4, while the diffusivity was dominated by the porosity of mixtures M2, M5, and M6, which were prepared with the highest content of PC and FA. Mixtures prepared with high portlandite content (M1, M3, M4) consistently had the lowest diffusivity throughout the 7-day period. In contrast, M5 (100% PC) decreased significantly by the 4th day of curing, which is expected due to its continued carbonation. M2 (50/50% FA/PC) increased to 2.85E-6 m^2/s (the highest of any mixture over the 7-day period) on the 4th day, but subsequently decreased on the 7th day. This fluctuation may be explained first by the low carbonation potential of FA, and second by the fluctuation of the pore saturation, which reached a minimum at 75% on the 4th day before increasing on the 7th day. Thus, it is proposed that carbonation is the greatest mechanism in impacting diffusivity for high calcium mixtures as with portlandite, while porosity and pore saturation begin to dominate in systems of low carbonation, such as fly ash. Portland cement is found to be an intermediate between the two mechanisms, likely depending significantly on the exact binder composition, water to binder ratio, and curing time.

For subsequent experiments, increasing the number of samples for each mixture and extending the curing time could significantly minimize the margin of error. Samples high in portlandite content such as M3 had the tendency to fracture or crumble, rendering them unfit for testing and requiring a new batch of the sample to be prepared. This may have led to an increase in error introduced in sample preparation. A large portion of sample preparation relied on mixing by hand and filling each mold manually, without any compressive loading. This may have led to inconsistencies in how tightly each sample was packed. The surfaces of the sample, although sealed by a lid, were not always smooth, which introduces error in the exact thickness of the

sample, and thus determination of the effective diffusion coefficient. Finally, preparation of additional mixtures of intermediate binder composition (e.g., 75/25% PC/FA) may provide a smoother ternary plot and understanding of the relationship between composition and the effective diffusion coefficient.

3.4: Thermogravimetric Analysis

As seen from Figure 3.4 and quantified in Table 3.4, the mixtures of the highest portlandite content (M1, M3, M4) had the greatest CO_2 uptake after diffusion, due to the abundance of CH available for carbonation to form $CaCO_3$. Between Portland cement and fly ash, the former is expected to have a higher CO_2 absorption capacity due to the initially present clinker phases, alite, belite, aluminate and ferrite, participating in the hydration reaction, leading to acceleration of the carbonation reaction and thus CO_2 uptake.

Table 3.4: Mass uptake (gCO_2/gBinder) for each sample and curing time

Cure\Mix	M1	M2	M3	M4	M5	M6
C1	0.023	0.120	0.095	0.249	0.125	0.053
C4	0.154	0.060	0.157	0.246	0.036	0.004
C7	0.260	0.031	0.184	0.198	0.036	0.008

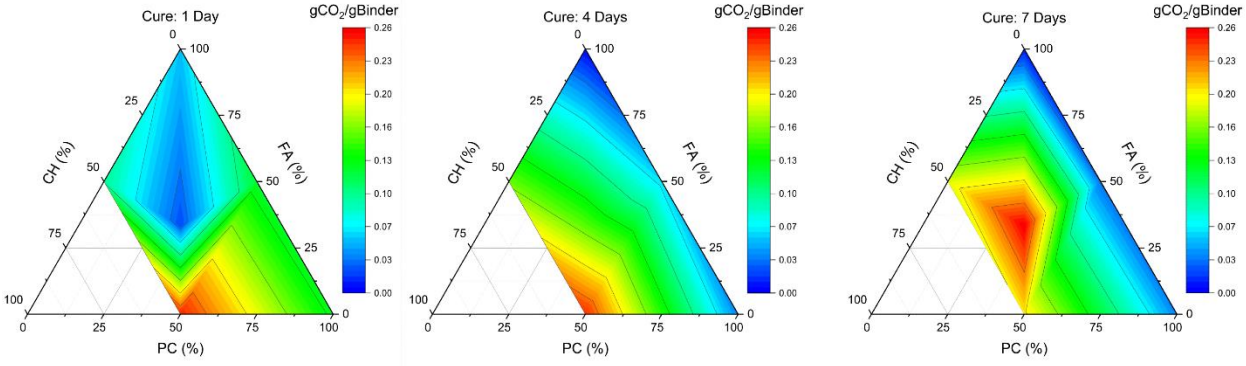

Figure 3.4: Ternary contour plot of CO_2 mass uptake

The results are consistent with this expectation, as M4 (50/50% PC/CH) showed the greatest CO_2 uptake at 0.249gCO_2/gBinder after 1 day of curing, with M3 only at 0.095gCO_2/gBinder. Following this, the high Portland cement content mixtures, M2 (50/50%

PC/FA) and M5 (100% PC) took 0.120gCO_2/gBinder and 0.125gCO_2/gBinder, respectively. M6 (100% FA) had the second-lowest CO_2 uptake at 0.053gCO_2/gBinder, greater only than M1 at 0.022gCO_2/gBinder. While a mixture of 100% CH was not tested, based on these results it can be reasonably predicted that a sample of 100% CH would have had the highest CO_2 uptake, as the trends across mixtures as well as over time support an increasing CO_2 uptake with the CH mixture content.

With increased curing time, the hydration reaction continues and an increase in carbonation with CH and CSH is expected. This expectation is met in M1 and M3 (50/50% FA/CH), which showed a consistent increase in CO_2 uptake after each curing period. M4 (50/50% PC/CH), the third of these three mixtures with high portlandite content, showed little change between 1 and 4 days of curing (0.003gCO_2/gBinder difference), but decreased by 0.048gCO_2/gBinder between 4 and 7 days of curing. In contrast, M2 (50/50% PC/FA), M5 (100% PC), and M6 (100% FA), the three mixtures made without added portlandite, all showed significant decreases between curing days 1 and 7, each ending with approximately a quarter of their original CO_2 uptake capacity.

Overall, these results are consistent with expected trends. While the exact values of CO_2 uptake were lower than expected, the trend of CH having the highest carbonation potential followed by PC and FA was observed. This also verifies the observed changes in carbonation potential determined from the diffusion and XRD tests.

CHAPTER 4: CONCLUSION

The carbonation of concrete was studied for a ternary binder system through tests by measuring CO_2 diffusion, determining concrete porosity and pore saturation, and carbonation phases of concrete over time with XRD and TGA. An experimental setup for measuring the diffusion coefficient was developed based on curve-fitting of Fick's second law. Multiple improvements to the diffusion chamber setup were discussed, and although these were not yet implemented due to time constraints, the results obtained from this setup were found to be consistent with literature values and were compared to the results for the four other tests noted above. For the three mixtures of 100% PC, 100% FA, and 50/50% PC/FA, the diffusion coefficient followed the expected trends of decreasing with decreasing porosity and increasing pore saturation. For mixtures with a high initial content of portlandite, the diffusion coefficient followed the expected trend of decreasing with increasing carbonation potential. This suggests that carbonation is the most significant mechanism impacting the effective diffusion coefficient, followed by porosity and pore saturation contributing less.

REFERENCES

[1] K. L. Scrivener, V. M. John, and E. M. Gartner, "Eco-efficient cements: Potential economically viable solutions for a low-CO2 cement-based materials industry," *Cem. Concr. Res.*, vol. 114, pp. 2–26, Dec. 2018, doi: 10.1016/j.cemconres.2018.03.015.

[2] C. Le Quéré *et al.*, "Global Carbon Budget 2018," *Earth Syst. Sci. Data*, vol. 10, no. 4, pp. 2141–2194, Dec. 2018, doi: 10.5194/essd-10-2141-2018.

[3] P. Friedlingstein *et al.*, "Global Carbon Budget 2020," *Earth Syst. Sci. Data*, vol. 12, no. 4, pp. 3269–3340, Dec. 2020, doi: 10.5194/essd-12-3269-2020.

[4] "CO2 uptake in cement-containing products".

[5] J. S. Damtoft, J. Lukasik, D. Herfort, D. Sorrentino, and E. M. Gartner, "Sustainable development and climate change initiatives," *Cem. Concr. Res.*, vol. 38, no. 2, pp. 115–127, Feb. 2008, doi: 10.1016/j.cemconres.2007.09.008.

[6] K. Humphreys and M. Mahasenan, "Towards a sustainable cement industry. Substudy 8: climate change," Mar. 2002, Accessed: Sep. 04, 2023. [Online]. Available: https://www.osti.gov/etdeweb/biblio/20269589

[7] "Cement," *IEA*. https://www.iea.org/energy-system/industry/cement (accessed Sep. 04, 2023).

[8] "PCA Projects Decline of Cement Demand for 2023," *For Construction Pros*, Oct. 17, 2022. https://www.forconstructionpros.com/concrete/press-release/22498793/portland-cement-association-pca-projects-decline-of-cement-demand-for-2023 (accessed Sep. 04, 2023).

[9] "Carbonation of concrete." https://www.ivl.se/projektwebbar/co2-concrete-uptake/carbonation-of-concrete.html (accessed Jul. 23, 2023).

[10] K.-H. Yang, E.-A. Seo, and S.-H. Tae, "Carbonation and CO2 uptake of concrete," *Environ. Impact Assess. Rev.*, vol. 46, pp. 43–52, Apr. 2014, doi: 10.1016/j.eiar.2014.01.004.

[11] S. Kashef-Haghighi, Y. Shao, and S. Ghoshal, "Mathematical modeling of CO 2 uptake by concrete during accelerated carbonation curing," *Cem. Concr. Res.*, vol. 67, pp. 1–10, Jan. 2015, doi: 10.1016/j.cemconres.2014.07.020.

[12] H. M. Saleh and S. B. Eskander, "Innovative cement-based materials for environmental protection and restoration," in *New Materials in Civil Engineering*, Elsevier, 2020, pp. 613–641. doi: 10.1016/B978-0-12-818961-0.00018-1.

[13] J. Marchand, D. P. Bentz, E. Samson, and Y. Maltais, "Influence of Calcium Hydroxide Dissolution on the Transport Properties of Hydrated Cement Systems," *NIST*, Jan. 2001, Accessed: Jul. 23, 2023. [Online]. Available: https://www.nist.gov/publications/influence-calcium-hydroxide-dissolution-transport-properties-hydrated-cement-systems

[14] M. Castellote and C. Andrade, “Modelling the carbonation of cementitious matrixes by means of the unreacted-core model, UR-CORE,” *Cem. Concr. Res.*, vol. 38, no. 12, pp. 1374–1384, Dec. 2008, doi: 10.1016/j.cemconres.2008.07.004.

[15] T. Yang, B. Keller, E. Magyari, K. Hametner, and D. Günther, “Direct observation of the carbonation process on the surface of calcium hydroxide crystals in hardened cement paste using an Atomic Force Microscope,” *J. Mater. Sci.*, vol. 38, no. 9, pp. 1909–1916, May 2003, doi: 10.1023/A:1023544228319.

[16] D. Zhang, Z. Ghouleh, and Y. Shao, “Review on carbonation curing of cement-based materials,” *J. CO2 Util.*, vol. 21, pp. 119–131, Oct. 2017, doi: 10.1016/j.jcou.2017.07.003.

[17] A. Fabbri *et al.*, “Effect of carbonation on the hydro-mechanical properties of Portland cements,” *Cem. Concr. Res.*, vol. 39, no. 12, pp. 1156–1163, Dec. 2009, doi: 10.1016/j.cemconres.2009.07.028.

[18] J. Jerga, “Physico-mechanical properties of carbonated concrete,” *Constr. Build. Mater.*, vol. 18, no. 9, pp. 645–652, Nov. 2004, doi: 10.1016/j.conbuildmat.2004.04.029.

[19] J. Xiao, J. Li, B. Zhu, and Z. Fan, “Experimental study on strength and ductility of carbonated concrete elements,” *Constr. Build. Mater.*, vol. 16, no. 3, pp. 187–192, Apr. 2002, doi: 10.1016/S0950-0618(01)00034-4.

[20] B. Šavija and M. Luković, “Carbonation of cement paste: Understanding, challenges, and opportunities,” *Constr. Build. Mater.*, vol. 117, pp. 285–301, Aug. 2016, doi: 10.1016/j.conbuildmat.2016.04.138.

[21] “Supplementary Cementing Materials.” https://www.cement.org/cement-concrete/concrete-materials/supplementary-cementing-materials (accessed Sep. 06, 2023).

[22] “Standard Specification for Coal Fly Ash and Raw or Calcined Natural Pozzolan for Use in Concrete.” https://www.astm.org/c0618-22.html (accessed Aug. 30, 2023).

[23] “Standard Specification for Slag Cement for Use in Concrete and Mortars.” https://www.astm.org/c0989_c0989m-18a.html (accessed Sep. 07, 2023).

[24] “Standard Specification for Silica Fume Used in Cementitious Mixtures.” https://www.astm.org/c1240-20.html (accessed Sep. 07, 2023).

[25] “Standard Guide for Evaluation of Alternative Supplementary Cementitious Materials (ASCM) for Use in Concrete.” https://www.astm.org/c1709-18.html (accessed Sep. 06, 2023).

[26] Y. Han, R.-S. Lin, and X.-Y. Wang, “Compressive Strength Estimation and CO2 Reduction Design of Fly Ash Composite Concrete,” *Buildings*, vol. 12, no. 2, Art. no. 2, Feb. 2022, doi: 10.3390/buildings12020139.

[27] A. Mazzella, M. Errico, and D. Spiga, “CO2 uptake capacity of coal fly ash: Influence of pressure and temperature on direct gas-solid carbonation,” *J. Environ. Chem. Eng.*, vol. 4, no. 4, pp. 4120–4128, Dec. 2016, doi: 10.1016/j.jece.2016.09.020.

[28] R. Kurda, J. De Brito, and J. D. Silvestre, “Carbonation of concrete made with high amount of fly ash and recycled concrete aggregates for utilization of CO2,” *J. CO2 Util.*, vol. 29, pp. 12–19, Jan. 2019, doi: 10.1016/j.jcou.2018.11.004.

[29] “Chapter 3 - Fly Ash in Portland Cement Concrete - Fly Ash Facts for Highway Engineers - Recycling - Sustainability - Pavements - Federal Highway Administration.” https://www.fhwa.dot.gov/pavement/recycling/fach03.cfm (accessed Aug. 29, 2023).

[30] B. Lothenbach, K. Scrivener, and R. D. Hooton, “Supplementary cementitious materials,” *Cem. Concr. Res.*, vol. 41, no. 12, pp. 1244–1256, Dec. 2011, doi: 10.1016/j.cemconres.2010.12.001.

[31] “Chapter 1 - Fly Ash - An Engineering Material - Fly Ash Facts for Highway Engineers - Recycling - Sustainability - Pavements - Federal Highway Administration.” https://www.fhwa.dot.gov/pavement/recycling/fach01.cfm (accessed Aug. 28, 2023).

[32] Building and Construction Department, Technical College of Mosul, Iraq, *Esra’a Abdul Salam Mahmood, M. Adnan Basher, Building and Construction Department, Technical College of Mosul, Iraq, A. Zeki Saber Agha, and Civil Department, Erbil Technical Engineering College, Erbil Polytechnic University Erbil, Iraq, “EFFECTE OF FLY ASH AS A SUSTAINABLE MATERIAL ON LIGHTWEIGHT FOAMED CONCRETE MIXES,” *J. Eng. Sustain. Dev.*, vol. 22, no. 02, pp. 108–124, Mar. 2018, doi: 10.31272/jeasd.2018.2.54.

[33] “ASTM C618 Fly Ash Specification: Comparison with Other Specifications, Shortcomings, and Solutions,” *ACI Mater. J.*, vol. 118, no. 1, Jan. 2021, doi: 10.14359/51725994.

[34] Z. Tafheem, S. Khusru, and S. Nasrin, “Environmental Impact of Green Concrete in Practice,” Dec. 2011.

[35] *Read “Gaseous Carbon Waste Streams Utilization: Status and Research Needs” at NAP.edu*. doi: 10.17226/25232.

[36] K. Vance, G. Falzone, I. Pignatelli, M. Bauchy, M. Balonis, and G. Sant, “Direct Carbonation of Ca(OH)2 Using Liquid and Supercritical CO2: Implications for Carbon-Neutral Cementation,” *Ind. Eng. Chem. Res.*, vol. 54, no. 36, pp. 8908–8918, Sep. 2015, doi: 10.1021/acs.iecr.5b02356.

[37] B. Gilroy, L. Black, D. Thompson, R. Hogan, and N. Holmes, “Effects of Accelerated Carbonation Curing on CO2 Sequestration and on the Compressive Strength of Concrete Masonry Units,” *Conf. Pap.*, Aug. 2020, [Online]. Available: https://arrow.tudublin.ie/engschcivcon/136

[38] R. Loser, B. Lothenbach, A. Leemann, and M. Tuchschmid, “Chloride resistance of concrete and its binding capacity – Comparison between experimental results and thermodynamic modeling,” *Cem. Concr. Compos.*, vol. 32, no. 1, pp. 34–42, Jan. 2010, doi: 10.1016/j.cemconcomp.2009.08.001.

[39] X. Liu, P. Feng, Y. Cai, X. Yu, C. Yu, and Q. Ran, “Carbonation behavior of calcium silicate hydrate (C-S-H): Its potential for CO2 capture,” *Chem. Eng. J.*, vol. 431, p. 134243, Mar. 2022, doi: 10.1016/j.cej.2021.134243.

[40] J. J. Chen, J. J. Thomas, and H. M. Jennings, “Decalcification shrinkage of cement paste,” *Cem. Concr. Res.*, vol. 36, no. 5, pp. 801–809, May 2006, doi: 10.1016/j.cemconres.2005.11.003.

[41] P. Faucon *et al.*, “Leaching of cement: Study of the surface layer,” *Cem. Concr. Res.*, vol. 26, no. 11, pp. 1707–1715, Nov. 1996, doi: 10.1016/S0008-8846(96)00157-3.

[42] T. Thorvaldson, *Proceedings of the Third International Symposium of the Chemistry of Cement: London 1952 Chemical Aspects of the Durability of Cement Products*. Cement & Concrete Assoc., 1954.

[43] P. K. Mehta, “Mechanism of expansion associated with ettringite formation,” *Cem. Concr. Res.*, vol. 3, no. 1, pp. 1–6, Jan. 1973, doi: 10.1016/0008-8846(73)90056-2.

[44] W. Kunther, B. Lothenbach, and J. Skibsted, “Influence of the Ca/Si ratio of the C–S–H phase on the interaction with sulfate ions and its impact on the ettringite crystallization pressure,” *Cem. Concr. Res.*, vol. 69, pp. 37–49, Mar. 2015, doi: 10.1016/j.cemconres.2014.12.002.

[45] A. K. Crumbie, K. L. Scrivener, and P. L. Pratt, “The Relationship Between The Porosity And Permeability Of The Surface Layer Of Concrete And The Ingress Of Aggressive Ions,” *MRS Proc.*, vol. 137, p. 279, 1988, doi: 10.1557/PROC-137-279.

[46] K. L. Scrivener, J. F. Young, and Materials Research Society, Eds., *Mechanisms of chemical degradation of cement-based systems: proceedings of the Material Research Society’s Symposium on Mechanisms of Chemical Degradation of Cement-based Systems, Boston, USA, 27-30 November 1995*. London ; New York: E & FN Spon, 1997.

[47] V. Dutzer, W. Dridi, S. Poyet, P. Le Bescop, and X. Bourbon, “The link between gas diffusion and carbonation in hardened cement pastes,” *Cem. Concr. Res.*, vol. 123, p. 105795, Sep. 2019, doi: 10.1016/j.cemconres.2019.105795.

[48] C. Andrade and R. Buják, “Effects of some mineral additions to Portland cement on reinforcement corrosion,” *Cem. Concr. Res.*, vol. 53, pp. 59–67, Nov. 2013, doi: 10.1016/j.cemconres.2013.06.004.

[49] M. Merlini, G. Artioli, T. Cerulli, F. Cella, and A. Bravo, “Tricalcium aluminate hydration in additivated systems. A crystallographic study by SR-XRPD,” *Cem. Concr. Res.*, vol. 38, no. 4, pp. 477–486, Apr. 2008, doi: 10.1016/j.cemconres.2007.11.011.

[50] "is417 Ettringite Formation and the performance of concrete.pdf." Accessed: Aug. 28, 2023. [Online]. Available: https://www.cement.org/docs/default-source/fc_concrete_technology/is417-ettringite-formation-and-the-performance-of-concrete.pdf?sfvrsn=412%26sfvrsn=412

[51] Q. Yuan, Z. Liu, K. Zheng, and C. Ma, "Inorganic cementing materials," in *Civil Engineering Materials*, Elsevier, 2021, pp. 17–57. doi: 10.1016/B978-0-12-822865-4.00002-7.

[52] "globe_sp05_spec_sheet.pdf." Accessed: Aug. 30, 2023. [Online]. Available: https://globefoodequip.com/pdfs/doc-lib/mixers/globe_sp05_spec_sheet.pdf

[53] A. Khitab, M. Arshad, and M. Munir, "Modelling of Chloride Diffusion through Concrete using Fick's laws of Diffusion," Oct. 2013.

[54] W. Gu, F. Xu, S. Wang, W. Li, and Y. Tan, "Effect of Fly Ash Content on the Carbonization Resistance of Cement Paste," *IOP Conf. Ser. Earth Environ. Sci.*, vol. 153, p. 052042, May 2018, doi: 10.1088/1755-1315/153/5/052042.

[55] Y. F. Houst and F. H. Wittmann, "Influence of porosity and water content on the diffusivity of CO2 and O2 through hydrated cement paste," *Cem. Concr. Res.*, vol. 24, no. 6, pp. 1165–1176, 1994, doi: 10.1016/0008-8846(94)90040-X.

[56] F. Glasser, "Application of inorganic cements to the conditioning and immobilisation of radioactive wastes," in *Handbook of Advanced Radioactive Waste Conditioning Technologies*, Elsevier, 2011, pp. 67–135. doi: 10.1533/9780857090959.1.67.

[57] H. Cui, W. Tang, W. Liu, Z. Dong, and F. Xing, "Experimental study on effects of CO2 concentrations on concrete carbonation and diffusion mechanisms," *Constr. Build. Mater.*, vol. 93, pp. 522–527, Sep. 2015, doi: 10.1016/j.conbuildmat.2015.06.007.

[58] J. Zhang and G. W. Scherer, "Comparison of methods for arresting hydration of cement," *Cem. Concr. Res.*, vol. 41, no. 10, pp. 1024–1036, Oct. 2011, doi: 10.1016/j.cemconres.2011.06.003.

[59] L. Konecny and S. J. Naqvi, "The effect of different drying techniques on the pore size distribution of blended cement mortars," *Cem. Concr. Res.*, vol. 23, no. 5, pp. 1223–1228, Sep. 1993, doi: 10.1016/0008-8846(93)90183-A.

[60] H. F. W. Taylor and A. B. Turner, "Reactions of tricalcium silicate paste with organic liquids," *Cem. Concr. Res.*, vol. 17, no. 4, pp. 613–623, Jul. 1987, doi: 10.1016/0008-8846(87)90134-7.

[61] "Standard Specification for Woven Wire Test Sieve Cloth and Test Sieves." https://www.astm.org/e0011-22.html (accessed Sep. 01, 2023).

[62] Z. Zhang, J. Du, and M. Shi, “Quantitative Analysis of the Calcium Hydroxide Content of EVA-Modified Cement Paste Based on TG-DSC in a Dual Atmosphere,” *Materials*, vol. 15, no. 7, p. 2660, Apr. 2022, doi: 10.3390/ma15072660.

[63] K. De Weerdt, M. B. Haha, G. Le Saout, K. O. Kjellsen, H. Justnes, and B. Lothenbach, “Hydration mechanisms of ternary Portland cements containing limestone powder and fly ash,” *Cem. Concr. Res.*, vol. 41, no. 3, pp. 279–291, Mar. 2011, doi: 10.1016/j.cemconres.2010.11.014.

[64] A. S. Silva, A. Gameiro, J. Grilo, R. Veiga, and A. Velosa, “Long-term behavior of lime–metakaolin pastes at ambient temperature and humid curing condition,” *Appl. Clay Sci.*, vol. 88–89, pp. 49–55, Feb. 2014, doi: 10.1016/j.clay.2013.12.016.

[65] F. W. Wilburn, “Handbook of Thermal Analysis of Construction Materials,” *Thermochim. Acta*, vol. 406, no. 1–2, p. 249, Nov. 2003, doi: 10.1016/S0040-6031(03)00230-2.

[66] C. Andrade and M. Á. Sanjuán, “Carbon dioxide uptake by pure Portland and blended cement pastes,” *Dev. Built Environ.*, vol. 8, p. 100063, Sep. 2021, doi: 10.1016/j.dibe.2021.100063.

[67] “American Standard ASTM C150 Type1 Specification for Portland Cement.” http://www.tigercement.com/cement-products/ordinary-portland-cement/american-standard-astm-c-150-type-1/ (accessed Aug. 30, 2023).

[68] P. E. Stutzman, P. Feng, and J. W. Bullard, “Phase Analysis of Portland Cement by Combined Quantitative X-Ray Powder Diffraction and Scanning Electron Microscopy,” *J. Res. Natl. Inst. Stand. Technol.*, vol. 121, p. 47, Apr. 2016, doi: 10.6028/jres.121.004.

[69] A. A. Tabikh and R. J. Weht, “An X-ray diffraction analysis of portland cement,” *Cem. Concr. Res.*, vol. 1, no. 3, pp. 317–328, May 1971, doi: 10.1016/0008-8846(71)90006-8.

[70] Y. Yaping, Z. Xiaoqiang, Q. Weilan, and W. Mingwen, “Synthesis of pure zeolites from supersaturated silicon and aluminum alkali extracts from fused coal fly ash,” *Fuel*, vol. 87, no. 10–11, pp. 1880–1886, Aug. 2008, doi: 10.1016/j.fuel.2007.12.002.

[71] G. Wei, B. Dong, G. Fang, and Y. Wang, “Understanding reactive amorphous phases of fly ash through the acidolysis,” *Cem. Concr. Compos.*, vol. 140, p. 105102, Jul. 2023, doi: 10.1016/j.cemconcomp.2023.105102.

[72] “AMCSD Search Results - Gypsum.” http://rruff.geo.arizona.edu/AMS/minerals/Gypsum (accessed Aug. 28, 2023).

[73] R. T. Hemmings and E. E. Berry, “On the Glass in Coal Fly Ashes: Recent Advances,” *MRS Proc.*, vol. 113, p. 3, 1987, doi: 10.1557/PROC-113-3.

[74] P. T. Durdziński, R. Snellings, C. F. Dunant, M. B. Haha, and K. L. Scrivener, “Fly ash as an assemblage of model Ca–Mg–Na-aluminosilicate glasses,” *Cem. Concr. Res.*, vol. 78, pp. 263–272, Dec. 2015, doi: 10.1016/j.cemconres.2015.08.005.

[75] S. Kushwah, M. Mudgal, and R. K. Chouhan, “The Process, Characterization and Mechanical properties of fly ash-based Solid form geopolymer via mechanical activation,” *South Afr. J. Chem. Eng.*, vol. 38, pp. 104–114, Oct. 2021, doi: 10.1016/j.sajce.2021.09.002.

[76] J. L. Provis and J. S. J. Van Deventer, “Geopolymerisation kinetics. 2. Reaction kinetic modelling,” *Chem. Eng. Sci.*, vol. 62, no. 9, pp. 2318–2329, May 2007, doi: 10.1016/j.ces.2007.01.028.

[77] P. Duxson, A. Fernández-Jiménez, J. L. Provis, G. C. Lukey, A. Palomo, and J. S. J. Van Deventer, “Geopolymer technology: the current state of the art,” *J. Mater. Sci.*, vol. 42, no. 9, pp. 2917–2933, May 2007, doi: 10.1007/s10853-006-0637-z.

[78] A. Hajimohammadi, J. L. Provis, and J. S. J. van Deventer, “One-Part Geopolymer Mixes from Geothermal Silica and Sodium Aluminate,” *Ind. Eng. Chem. Res.*, vol. 47, no. 23, pp. 9396–9405, Dec. 2008, doi: 10.1021/ie8006825.

[79] H. A. Abdel Gawwad, S. Abd El-Aleem, and A. S. Ouda, “Preparation and characterization of one-part non-Portland cement,” *Ceram. Int.*, vol. 42, no. 1, Part A, pp. 220–228, Jan. 2016, doi: 10.1016/j.ceramint.2015.08.096.

[80] J. L. Provis, “4 - Activating solution chemistry for geopolymers,” in *Geopolymers*, J. L. Provis and J. S. J. van Deventer, Eds., in Woodhead Publishing Series in Civil and Structural Engineering. Woodhead Publishing, 2009, pp. 50–71. doi: 10.1533/9781845696382.1.50.

[81] “Standard Specification for Hydrated Lime for Masonry Purposes.” https://www.astm.org/c0207-18.html (accessed Sep. 02, 2023).

[82] R. Druteikienė, J. Šapolaitė, Ž. Ežerinskis, E. Naujalis, and A. Puzas, “Immobilization of radioactive waste in cement: Iodine binding by cementitious materials under highly alkaline conditions,” *Lith. J. Phys.*, vol. 55, no. 1, Apr. 2015, doi: 10.3952/physics.v55i1.3058.

[83] Munasir, Triwikantoro, M. Zainuri, and Darminto, “Synthesis of SiO_2 nanopowders containing quartz and cristobalite phases from silica sands,” *Mater. Sci.-Pol.*, vol. 33, no. 1, pp. 47–55, Mar. 2015, doi: 10.1515/msp-2015-0008.

[84] K. L. Scrivener, T. Füllmann, E. Gallucci, G. Walenta, and E. Bermejo, “Quantitative study of Portland cement hydration by X-ray diffraction/Rietveld analysis and independent methods,” *Cem. Concr. Res.*, vol. 34, no. 9, pp. 1541–1547, Sep. 2004, doi: 10.1016/j.cemconres.2004.04.014.

[85] M. L. Mings, S. M. Schlorholtz, J. M. Pitt, and T. Demirel, “Characterization of Fly Ash by X-Ray Analysis Methods”.

[86] “AMCSD Search Results - Ettringite.” http://rruff.geo.arizona.edu/AMS/minerals/Ettringite (accessed Aug. 28, 2023).

[87] N. J. Crammond, “Quantitative X-ray diffraction analysis of ettringite, thaumasite and gypsum in concretes and mortars,” *Cem. Concr. Res.*, vol. 15, no. 3, pp. 431–441, May 1985, doi: 10.1016/0008-8846(85)90116-4.

[88] H. C. Gran and E. W. Hansen, “Exchange rates of ethanol with water in water-saturated cement pastes probed by NMR,” *Adv. Cem. Based Mater.*, vol. 8, no. 3–4, pp. 108–117, Oct. 1998, doi: 10.1016/S1065-7355(98)00013-3.

[89] “Transport phenomena, R. B. Bird, W. E. Stewart, and E. N. Lightfoot, John Wiley and Sons, Inc., New York (1960). 780 pages. $11.50,” *AIChE J.*, vol. 7, no. 2, pp. 5J-6J, 1961, doi: 10.1002/aic.690070245.

[90] I.-S. Yoon and C.-H. Chang, “Time Evolution of CO2 Diffusivity of Carbonated Concrete,” *Appl. Sci.*, vol. 10, no. 24, p. 8910, Dec. 2020, doi: 10.3390/app10248910.

[91] N. Perez, *Electrochemistry and Corrosion Science*. Cham: Springer International Publishing, 2016. doi: 10.1007/978-3-319-24847-9.

[92] M. Daimon, T. Akiba, and R. Kondo, “Through Pore Size Distribution and Kinetics of the Carbonation Reaction of Portland Cement Mortars,” *J. Am. Ceram. Soc.*, vol. 54, no. 9, pp. 423–428, 1971, doi: 10.1111/j.1151-2916.1971.tb12379.x.

[93] G. R. Martin, “A method for determining the relative permeability of concrete using gas,” *Mag. Concr. Res.*, vol. 38, no. 135, pp. 90–94, Jun. 1986, doi: 10.1680/macr.1986.38.135.90.

[94] P. A. Claisse, H. El-Sayad, and I. G. Shaaban, “Permeability and pore volume of carbonated concrete,” *ACI Mater. J.*, vol. 96, no. 3, Art. no. 3, 1999.

[95] W. P. S. Dias, “Reduction of concrete sorptivity with age through carbonation,” *Cem. Concr. Res.*, vol. 30, no. 8, pp. 1255–1261, Aug. 2000, doi: 10.1016/S0008-8846(00)00311-2.

[96] H.-W. Song and S.-J. Kwon, “Permeability characteristics of carbonated concrete considering capillary pore structure,” *Cem. Concr. Res.*, vol. 37, no. 6, pp. 909–915, Jun. 2007, doi: 10.1016/j.cemconres.2007.03.011.

[97] S. H. Jung, M. K. Lee, and B. H. Oh, “Measurement Device and Characteristics of Diffusion Coefficient of Carbon Dioxide in Concrete,” *Mater. J.*, vol. 108, no. 6, pp. 589–595, Nov. 2011, doi: 10.14359/51683461.

[98] P. J. Dewaele, E. J. Reardon, and R. Dayal, “Permeability and porosity changes associated with cement grout carbonation,” *Cem. Concr. Res.*, vol. 21, no. 4, pp. 441–454, Jul. 1991, doi: 10.1016/0008-8846(91)90092-V.

[99] “Diffusion.” http://www.cco.caltech.edu/~brokawc/Bi145/Diffusion.html (accessed Sep. 08, 2023).

[100] J. Crank, *The mathematics of diffusion*, 2d ed. Oxford, [Eng]: Clarendon Press, 1975.

[101] I. L. Mostinsky, “DIFFUSION COEFFICIENT,” in *Thermopedia*, Begel House Inc., 2011. doi: 10.1615/AtoZ.d.diffusion_coefficient.

[102] W. Ashraf, “Carbonation of cement-based materials: Challenges and opportunities,” *Constr. Build. Mater.*, vol. 120, pp. 558–570, Sep. 2016, doi: 10.1016/j.conbuildmat.2016.05.080.

[103] H. Shi, B. Xu, T. Shi, and X. Zhou, “Determination of gas permeability of high performance concrete containing fly ash,” *Mater. Struct.*, vol. 41, no. 6, pp. 1051–1056, Jul. 2008, doi: 10.1617/s11527-007-9305-2.

[104] K. E. Hassan, J. G. Cabrera, and R. S. Maliehe, “The effect of mineral admixtures on the properties of high-performance concrete,” *Cem. Concr. Compos.*, vol. 22, no. 4, pp. 267–271, Jan. 2000, doi: 10.1016/S0958-9465(00)00031-7.